PENETRATION MECHANICS AND POST-PERFORATION EFFECTS IN AN ALUMINUM-ALUMINUM IMPACT SYSTEM

by

Marvin E. Backman
and
William J. Stronge

Research Department

ABSTRACT. The perforation of 0.040-, 0.125-, and 0.250-inch 2024-T3 aluminum alloy plates by 0.063-, 0.125-, and 0.281-inch 2024-T8 aluminum spheres are investigated for the impact velocity range from 1.0 to 4.0 km/sec. The object of the investigation is to determine the mechanism of the formation of fragments, the distribution of fragment velocities and sizes, and the relation of atmospheric disturbances to these properties of the fragment system. The projectiles are launched from a conventional powder gun and from a light-gas gun both of which are 0.5 inch in barrel diameter. The investigation uses an Electro-Optics Kerr cell camera, paraffin and celotex techniques of particle recovery, and measurements of momentum by a ballistic pendulum. Pressures of atmospheric disturbances are estimated from high-speed photographs of the shocks and directly by piezoelectric gages mounted in the top of a box to which the target plate is mounted. Pressure measurements are found to correlate in a general way to the kinetic energy of the particle system but show no significant contribution from the combustion of aluminum in air. The pressures from 0.125- and 0.040-inch targets are essentially the same.

NAVAL WEAPONS CENTER
CHINA LAKE, CALIFORNIA * OCTOBER 1967

NAVAL WEAPONS CENTER
AN ACTIVITY OF THE NAVAL MATERIAL COMMAND

M. R. Etheridge, Capt.,USN ..... Commander
H. G. Wilson ..... Technical Director (Acting)

FOREWORD

The material in this report represents part of a continuing applied research program in support of explosive ordnance problems at the Naval Weapons Center (formerly the U. S. Naval Ordnance Test Station). These studies were supported by funds under the Naval Air Systems Command Task Assignment A35-350-004/216-1/F008-08-06.

This report has been reviewed for technical accuracy by P. E. Cordle and R. G. S. Sewell.

Released by
HUGH W. HUNTER, Head
Research Department
9 August 1967

Under authority of
H. G. WILSON
Technical Director (Acting)

NWC Technical Publication 4414

Published by.....Research Department
Collation.....Cover, 30 leaves, DD Form 1473, abstract cards
First printing.....220 unnumbered copies
Security classification.....UNCLASSIFIED

CONTENTS

NOMENCLATURE

A_s	Cross sectional area of a sphere
C_D	Drag coefficient
C_H	Heat exchange coefficient
C_p	Specific heat of fragment material
D	Perforation diameter
d	Projectile diameter
h_f	Latent heat of fusion
h_v	Latent heat of vaporization
K	Drag constant
M	Plug mass
M_t	Target mass exclusive of plug
m	Projectile or fragment mass
m'	Mass ablated from fragment
q_i	Incident heat flux
q_m	Thermal energy of ablated material
s	Length
T	Temperature
t	Target plate thickness
V_r	Velocity after perforation
V_s	Initial projectile velocity
V_t	Velocity of target after perforation
ρ_a	Atmospheric density
ρ_p	Fragment density

INTRODUCTION

The impact of a projectile or a fragment against a plate at velocities of 2 km/sec or greater, and in which there is an extensive breakup of the impacting bodies, results in a significant pressure disturbance around the perforation exit. The pressure disturbances may be very intense at high velocities that can be attained by current weapons, for example by the fragments of a shaped-charge jet (approximately 2 to 10 km/sec). For this reason it is of interest in the analysis and improvement of weapons operations to better understand the details of the development of this kind of pressure disturbance and its correlation to the properties of the impact system. The present investigation is directed toward this end.

The work reported here continues an earlier investigation of the perforation of a plate and the formation of the fragment system. This investigation consists largely of photographic observations of the impact of explosively projected fragments and the examination of recovered fragments (Ref. 1-3). From these observations there emerges a qualitative picture of the impact irregularly shaped particles against plates of thickness comparable to the particle dimensions. In this picture the particle deforms extensively during penetration of the plate. The penetration itself is a local bulging of the plate that resembles the bursting of a bubble and is terminated by many, almost simultaneous, fractures of the bulged section. At the moment of bursting, the fragments are in a thin-shell configuration and continue to move as a thin shell of fragments until differences in interaction with the atmosphere from particle to particle have a noticeable effect.

The present work is an attempt to extend and improve these observations for irregularly shaped fragments. A sphere projected against a plate is chosen in order to obtain greater control over the impact conditions and to simplify the interpretation of experimental results. The light-gas gun is used for these studies and gives a range of impact velocities of approximately 0.2 km/sec to just under 4 km/sec. The spheres, with diameters of from 0.063 to 0.281 inch, are mounted in separating sabots and fired against plates of thicknesses from 0.040 to 0.250 inch. Both the spheres and plates are of aluminum alloys. The specific objectives are to determine the mechanism of the perforation of the plate and the formation of fragments, to determine the characteristics of the system of the fragments expelled from the plate, and to correlate the disturbances that result to the characteristics of the fragment system.

PERFORATION AND FRAGMENT FORMATION

PERFORATION PROCESS

Considerable information on the process of perforation can be obtained by the straightforward method of firing spheres against plates for a range of impact velocities and then examining the craters, the recovered projectiles, and the recovered fragments. Photographs of cross-sections of two series of perforations and the corresponding major recovered fragments are shown in Fig. 1. Figure 1 shows the dependence of perforation diameter on the projectile deformation. Deformation begins by flattening of the projectile. As the sides flow radially they are swept back, forming a cup. The walls of the cup eventually break off and contribute to the mass of smaller fragments in the fragment system. (After one firing against a 0.250-inch-thick target, shown in Fig. 1, the base of such a projectile cup and a separate ring that had composed the walls were recovered. The inner wall of this cup, which was the rear hemispherical surface of the original sphere, showed no abrasion or surface fracturing.) These studies of projectile deformation indicate that the effect of increasing the ratio of plate thickness to sphere diameter is to increase the time during which the projectile is deforming. As long as the projectile remains intact it asymptotically approaches a steady-state nose radius and body diameter that depend upon the perforation velocity and the initial diameter. The perforation will also asymptotically approach a limiting diameter with increasing plate thickness as long as the impact velocity is much greater than the minimum perforation velocity and reduction of velocity during perforation can be neglected. If the impact velocity is only slightly above the minimum perforation velocity, the projectile velocity will be appreciably reduced during penetration with the result that the exit perforation diameter is also reduced.

The perforation diameters are measured as the average minimum crater dimension. These data are plotted in Fig. 2 and 3 in the form of the ratio of hole diameter to projectile diameter as a function of impact velocity. Figure 2 shows this relation for 0.281-inch-diameter spheres and three target thicknesses. Figure 3 shows comparable data for two sphere diameters. These data increase linearly with increasing impact velocity and in this respect are in agreement with the result of Maiden (Ref. 4). Maiden's data went to almost double the maximum velocity achieved here and were obtained for projectile/plate systems that had a plate-thickness-to-projectile-diameter ratio of less than 0.504. Maiden's data fitted the empirical relation

$$D/d = 0.45\ V(t/d)^{2/3} + 0.90$$

The data in Fig. 2 do not show the constant 0.90 but rather a monotonically decreasing term with increasing plate thickness. This is probably due to the greater change in velocity with increasing plate thickness so that, at any given velocity, the thick target causes a greater

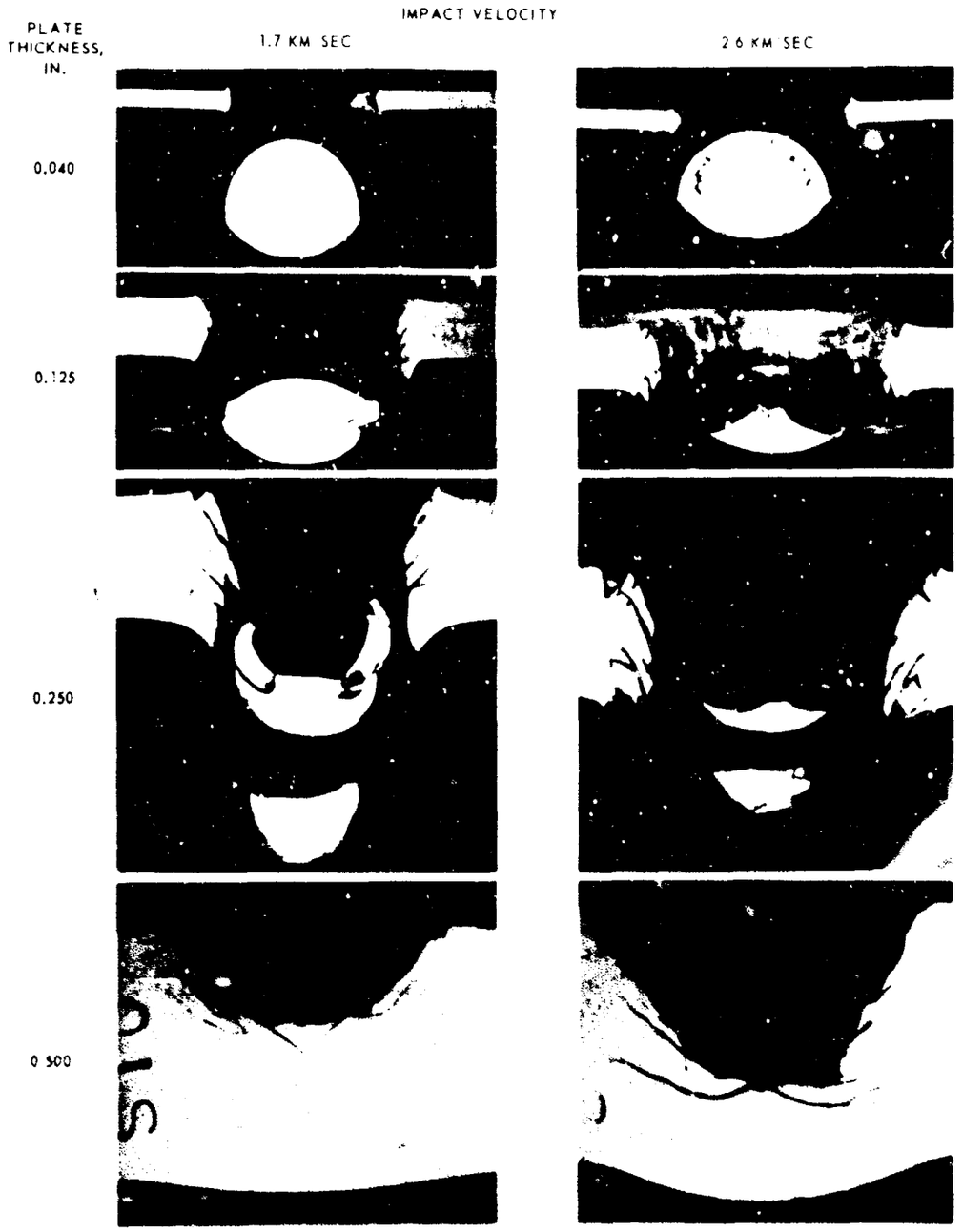

FIG. 1. Cross Sections of Two Series of Perforations at 1.7 km/sec and 2.6 km/sec.

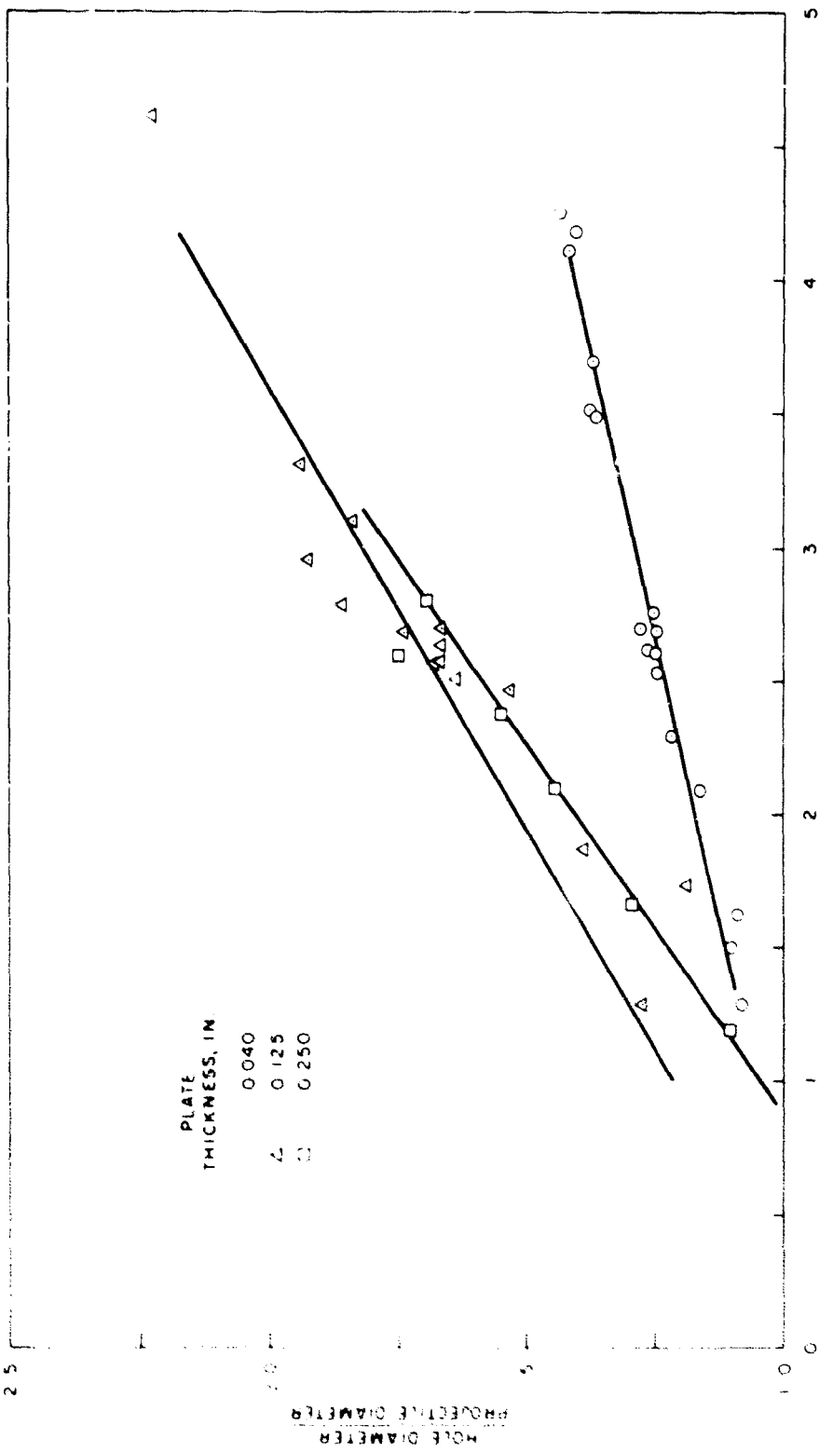

FIG. 2. Perforations of Aluminum Plates by 0.281-in. Diameter Aluminum Spheres.

variation in the projectile velocity during penetration than does a thin target. Also, comparing the data taken from 0.125- and 0.281-inch-diameter spheres, the perforation-to-sphere-diameter ratio is not independent of the projectile diameter. The smaller spheres increase the value of the constant 0.90 and decrease the coefficient of the velocity dependent term.

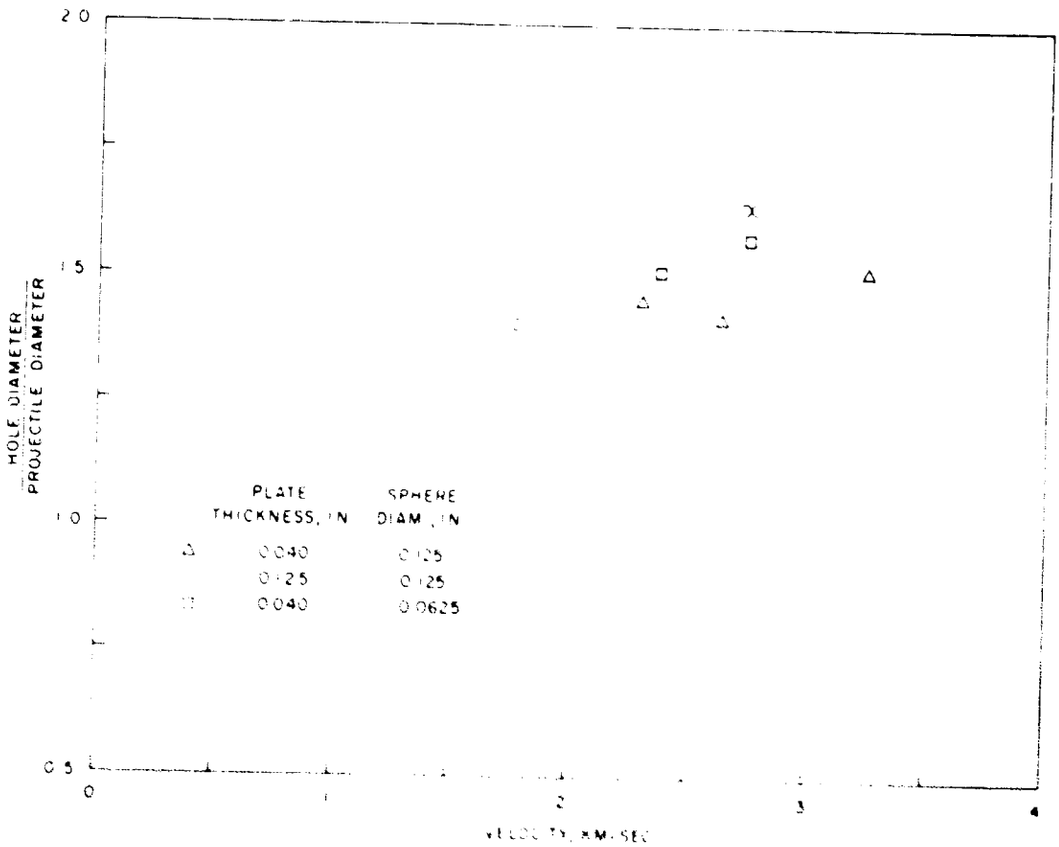

FIG. 3. Perforations of Aluminum Plates by Aluminum Spheres.

Halperson (Ref. 5) also has obtained data on 2024 aluminum alloy plates perforated by 0.1875-inch-diameter aluminum spheres at 5.74 km/sec. These impact systems had a ratio of plate thickness to projectile diameter of unity and the ratios of perforation diameter to projectile diameter had a maximum value of 3.5. Greater plate thicknesses result in decreasing perforation diameters.

A few tests in which 0.281-inch-diameter spheres perforated 6061-T6 plates resulted in holes that are slightly larger than shown in Fig. 2. This aluminum alloy has approximately 75% of the yield strength of

2024-T3; hence, material strength may also be a pertinent parameter in determining the perforation diameter. Although current empirically determined perforation diameter formulas do not include these variables, more complicated empirical expressions are not warranted without further analytical development or a much more intensive experimental program.

FRAGMENT FORMATION

In order to obtain information on the dynamics of fragment formation the impact event is photographed by means of an electro-optical camera with a Kerr cell shutter. The fragments are also recovered in foam, cotton, and fiberboard from which data it is possible to get significant detail on the basic mechanism of fragment formation. Witness plates are used to get data on the spatial distribution of the particles of various sizes. The qualitative picture of fragment formation and motion that is obtained for the sphere-plate system is much the same as that for the explosively projected particles

Among the recovered fragments it is usually possible to recognize a part of the original sphere that has been deformed in varying extents depending on the plate thickness. A deformed projectile that retains 95% of its original mass can be seen emerging from the fragment cloud in Fig. 4. In the range of velocities that has been investigated, the diameter of the perforation in the plate is less than a millimeter larger than the diameter of the recovered projectiles so that the hole size is apparently controlled by the deformation of the projectile.

A probable source of extensive projectile fragmentation in high velocity impacts are the internal multiple spall-type fractures apparent in the projectile shown in Fig. 1 that has perforated the 0.040-inch-thick plate at 2.6 km/sec. Initially, this type of fracture will only result in the early loss of the walls of the deformed projectile cup. This behavior leaves the base of the cup as the only major fragment in the 0.125-inch-thick, 2.6-km/sec example. The same result is eminent in the 0.250-inch-thick, 1.7-km/sec specimen. As the impact velocity and the pressures on the system increase, this type of fracturing becomes more extensive. Witness plates beyond the thin-plate target reveal that there are no longer any major fragments of either projectile or plate when the impact velocity exceeds 3.4 km/sec with plates up to 0.250-inch thick.

In addition to the projectile, large fragments of the plate are also identified among the recovered fragments. The largest of these generally consist of truncated cone plugs from the center of the impact area as depicted for 0.250-inch plates in Fig. 1. These plugs, which have a large base coinciding with the impact interface and a small base with the rear surface of the plate, are characteristic of impacts in which the plate thickness is comparable with the sphere diameter. They appear to

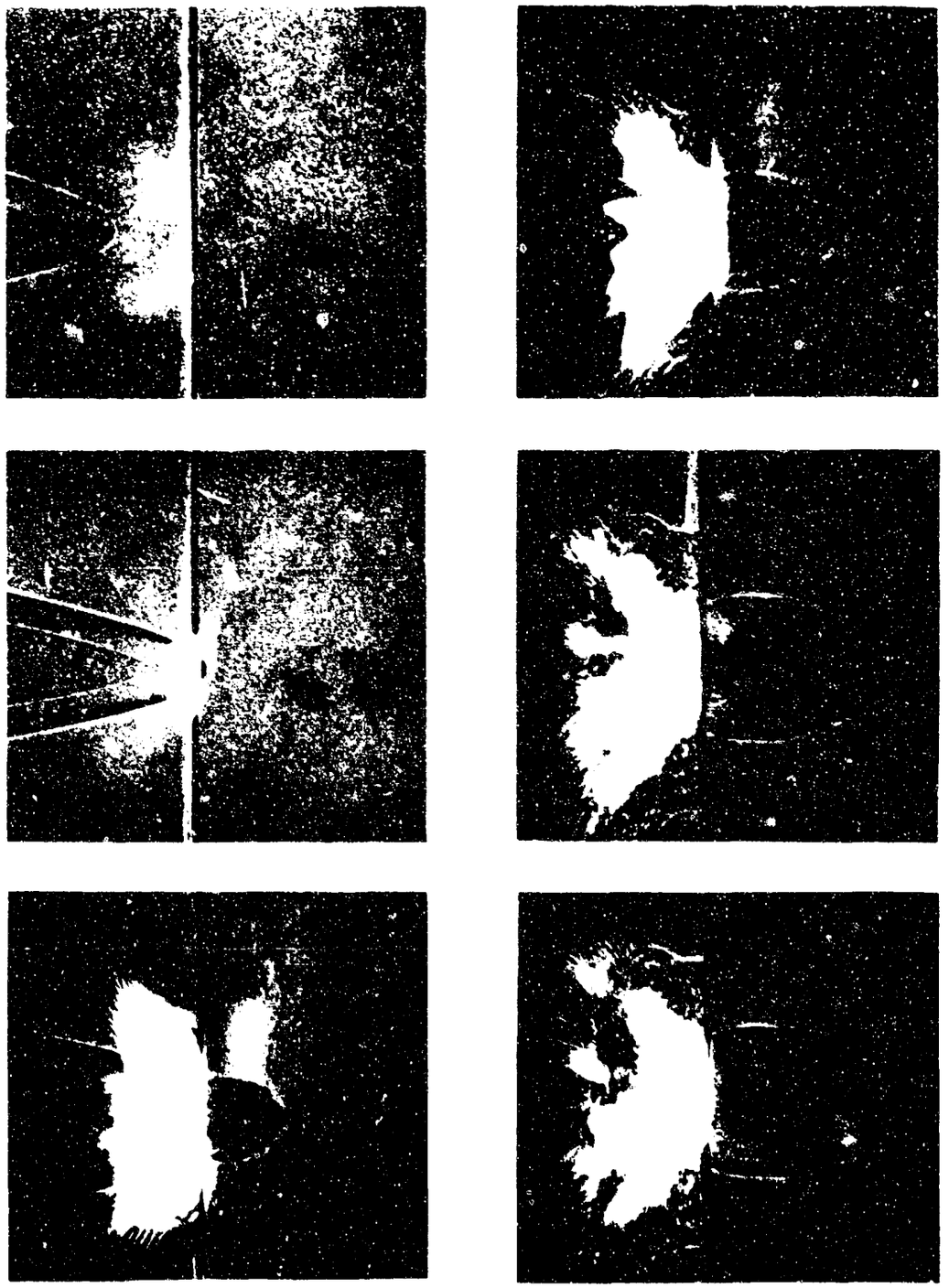

FIG. 4. Six Photographs of a Sphere Perforating a 0.040-in. Aluminum Alloy Plate at 4 km/sec.

result from conchoidal fractures occurring along lines of maximum shear stress; there are no indications of spalling in these plugs. In general, the size decreases with increasing impact velocity. Plugs such as these are typical of impacts of blunt projectiles with thick targets as shown in Ref. 1 but are somewhat unexpected for spherical projectiles and thin targets.

CHARACTERISTICS OF THE FRAGMENT SYSTEM

MASS DISTRIBUTION

The characteristics of the fragment system that are of the most interest in the consideration of energy transfer to the atmosphere are the distribution of fragment sizes, or masses, and the distribution of fragment velocities. The fragments with micron- to millimeter-size diameters are of greater importance to the various energy transfer theories than the major fragments.

The data from three tests in which fragments are collected in paraffin beyond the target plate are shown in Table 1. The particles are separated from the collection medium by melting the paraffin and pouring it through a #400 sieve. Other U. S. Standard Sieve Series screens are used to divide the collected particles into rough-size categories. A measure of the average particle size collected on the finer screens is made by microscopically measuring Martin's diameter on a sample consisting of 100 to 200 fragments. Martin's diameter is the horizontal dimension across the midpoint of the particle lying in a random orientation (Ref. 6). These data are normalized for direct comparison with other mass distribution data by determining the percentage of the total recovered mass that remains on each screen. By using this figure with an estimate of the average range of particle diameters collected in each sieve, a mass density distribution function is constructed (Fig. 5). This function is analogous to a spectral density function in which the argument is particle diameter.

Along with the averages of the data shown in Table 1, Fig. 5 contains results reported by Becker and Vitali (Ref. 7) and earlier results of Backman (Ref. 3). Both of these studies used explosively projected pellets with an impact velocity around 3.2 km/sec. The first of these had plates of 2S-0 aluminum and a water-collection technique while Backman, using 2024-T6 plates, calculated the particle size from witness-plate crater dimensions after measuring the fragment field velocities. All of these results show that only a small percentage of the total recovered fragment mass has particle diameters less than 400 microns. The percentage of tiny particles does increase with decreasing plate thickness. There is little likelihood that any significant percentage of particles were lost by passing through the #400 screen, since the mass density

distribution function seems to decrease monotonically with decreasing particle size. It is disconcerting to note, however, that except for the thinnest plates, the recovery techniques reported here and in Ref. 3 captured no more than two-thirds of the expected fragment mass; i.e., the projectile mass plus the mass missing from the target plate.

TABLE 1. Fragment Mass Distribution Measurements

Plate thickness			0.040 in.	0.125 in.	0.125 in.
Impact velocity			1.9 km/sec	3.16 km/sec	3.7 km/sec
Sieve no.	Opening, μ	Martin's diam., μ	Mass, mg	Mass, mg	Mass, mg
60	250	...	625	669	855
100	149	293	20	3	18
140	105	180	8	2.5	5.5
200	74	120	...	1.2	9
Pan	...	...	4	2.5	9
Total recovered mass			657	678.2	896.5
Projectile and missing target mass			...	1540	1623

A comment is in order on fragment sizes obtained for other projectile shapes. There have been several tests in which cylinders with a length-to-diameter ratio of around one were impacted against thin plates at normal incidence. Even with the thinnest plates and lowest perforation velocities, there were never any large fragments that could be identified with particular parts of the impact system. Apparently, the superior energy coupling between the flat surfaces resulted in extensive spallation in both the plate and the projectile. Although this effect of projectile geometry on the fragment size distribution should be studied further, spheres and Pugh pellets probably represent the effects of shaped-charge-particle impacts more closely than do the cylinders.

SPATIAL DISTRIBUTION OF FRAGMENT VELOCITIES

Sophisticated estimates of the energy partition following perforation will depend upon information on the spatial distribution of fragments and the distribution of fragment velocities throughout the field. Some data of this type were previously reported from tests in which explosively projected pellets were fired against 0.125-inch-thick 2024-T3 plates (Ref. 3). Qualitatively, it was observed that the fragment forms an expanding shell.

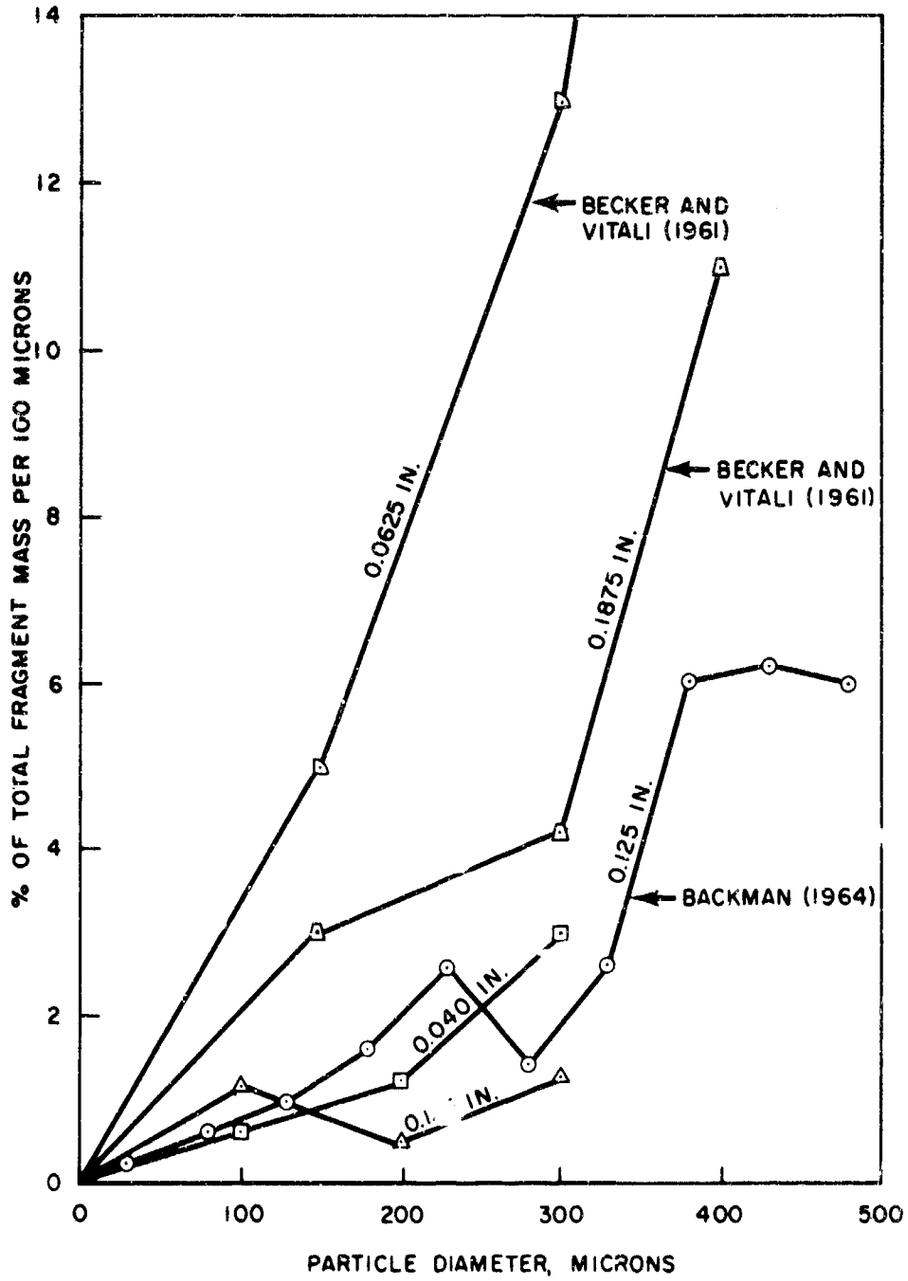

FIG. 5. Spectral Density Distribution of the Fragment Mass at Small Particle Sizes as a Function of the Plate Thickness.

In general, thin targets result in a more uniform fragment velocity than do thicker targets. Following the main mass of fragments, the thick plate often has large and relatively slow particles that travel along the sides of the volume swept out by the fragment field.

Information on the angular distribution of fragments, which included target thickness as one of the variables, was reported by Becker and Vitali (Ref. 7). These measurements show that 0.063-, 0.125-, and 0.1875-inch-thick 2024-T3 plates all have over 50% of the total number of fragments within 20 degrees of the fragment velocity field centerline and 95% within 40 degrees. A celotex-backed, foil, witness plate located roughly 25 perforation diameters behind the target was used to make these measurements. In the present studies of the impact of spheres against plates, data on the distribution of the fragment velocities as a function of the angular location of the fragments are obtained from photographic records taken by a six-frame Kerr cell camera. Each datum is obtained by measuring the change in location of a particle at the edge of the two-dimensional view of the fragment pattern. This is done to reduce the errors inherent in the use of the two-dimensional representation of the three-dimensional distribution. These data are presented in Fig. 6-15 as the discrete points. Each of these points shows the magnitude of the velocity of a particle that in the first frame has the given angular location with respect to the point defined by the intersection of the plane rear surface of the target and line of flight of the sphere.

The solid lines in Fig. 6-15 are the function $V = V_0 \cos(2\theta)$ with the value of V_0 chosen to fit the data points. It can be seen that this simple formula serves reasonably well as an empirical relation between velocity and the angle of emergence of the particles. There is a consistent departure of the data from this empirical relation at the higher angles of emergence.

FRAGMENT VELOCITY CALCULATION

The usual models of plate perforation consist of plugging, petaling, spalling, and ductile hole enlargement. In the present experiments, the perforations, the major fragments that are recovered, and the observations of relative fragment velocities all support the plugging mode of plate failure. A mathematical model of plugging is used that applies the conservation of momentum to a system of components whose behavior is constrained by simplifying assumptions. Foremost among these is the assumption that the entire mass of both the projectile and the material removed from the plate (the plug) have the same velocity following perforation. If one then includes the momentum acquired by the target during perforation the relationship between the initial and final momentum of the system will be

$$mV_s = (m + M)V_r + M_t V_t \qquad (1)$$

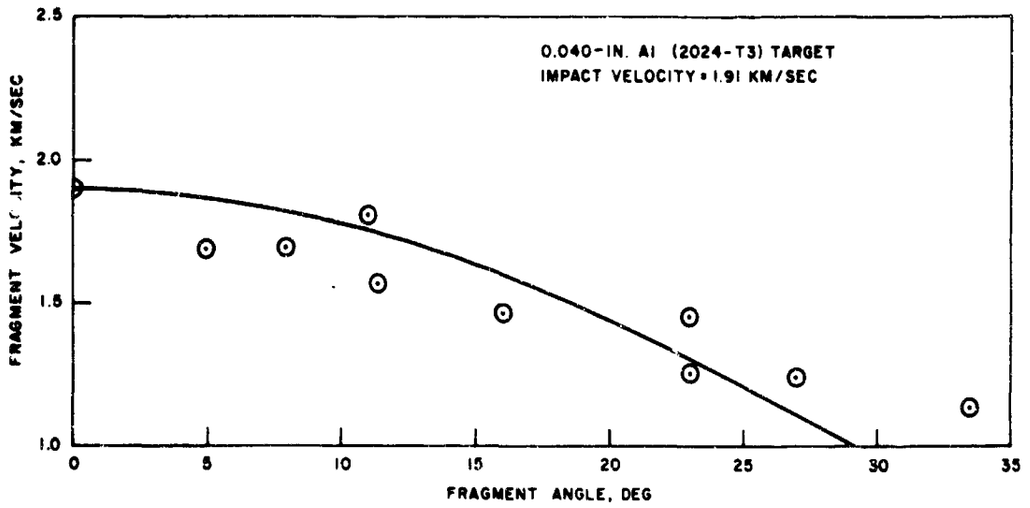

FIG. 6. Fragment Velocity Against Angle of Motion.

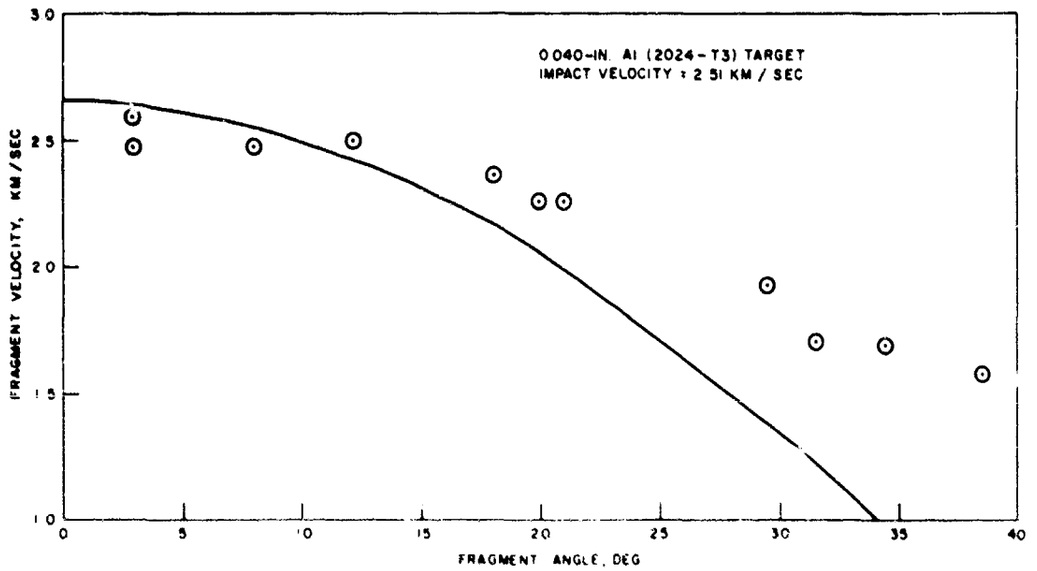

FIG. 7. Fragment Velocity Against Angle of Motion.

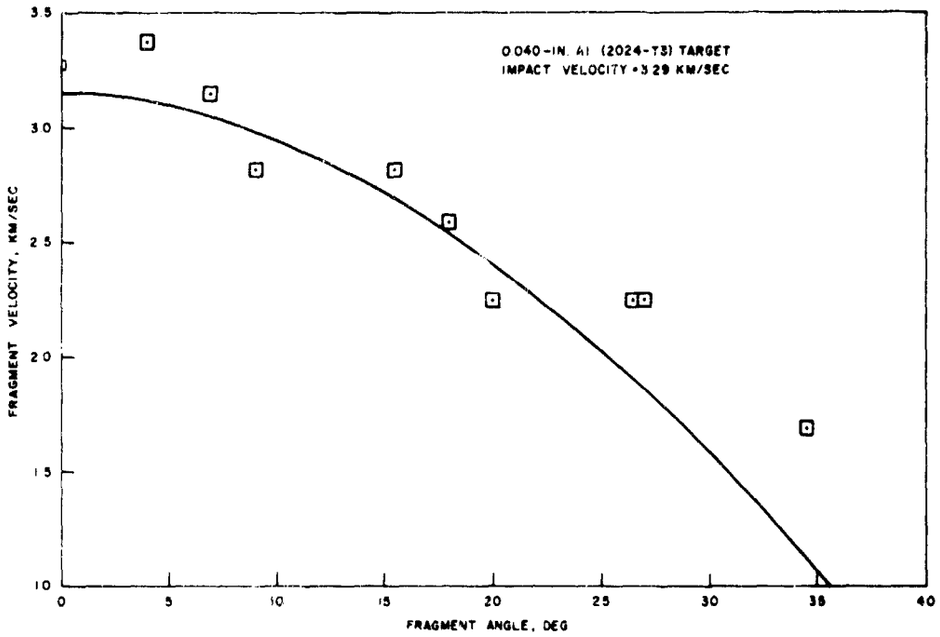

FIG. 3. Fragment Velocity Against Angle of Motion.

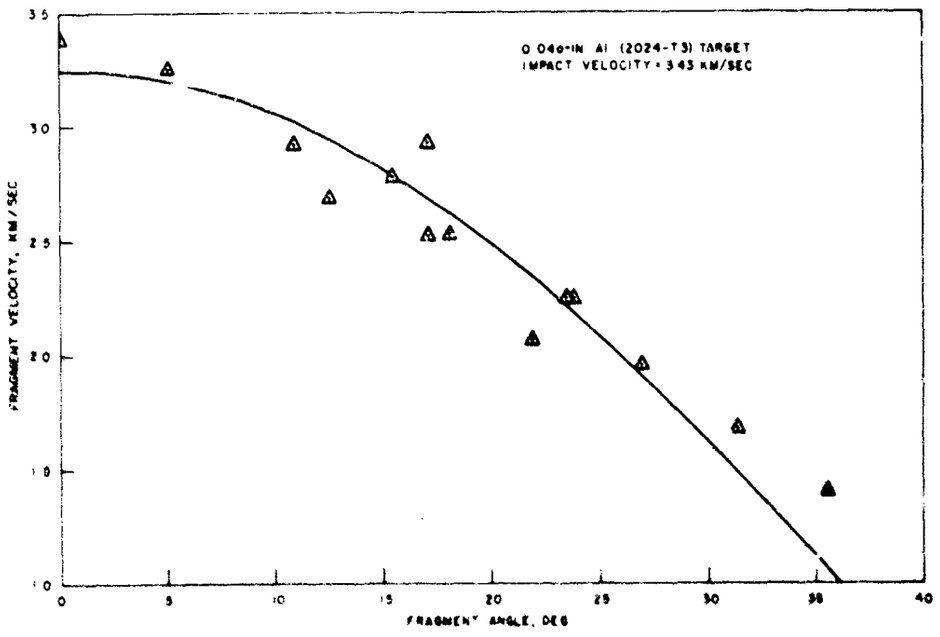

FIG. 9. Fragment Velocity Against Angle of Motion.

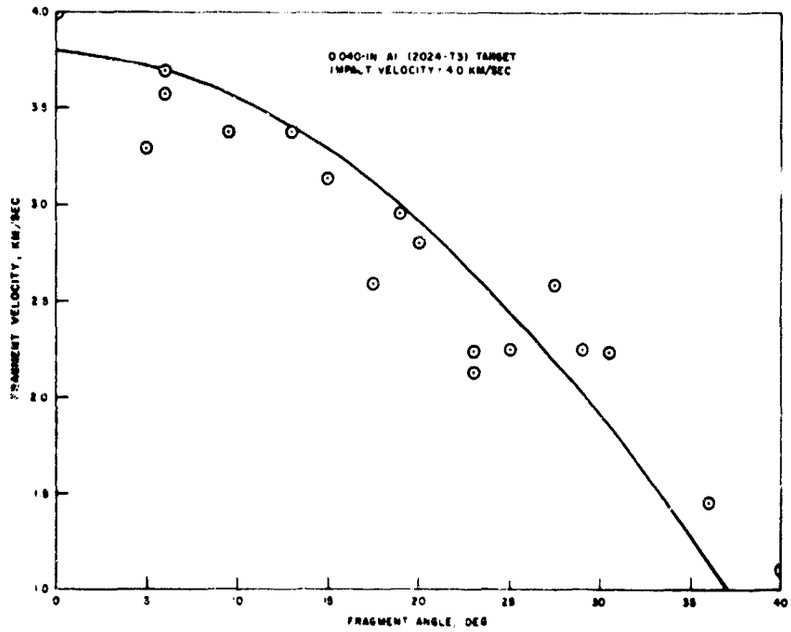

FIG. 10. Fragment Velocity Against Angle of Motion.

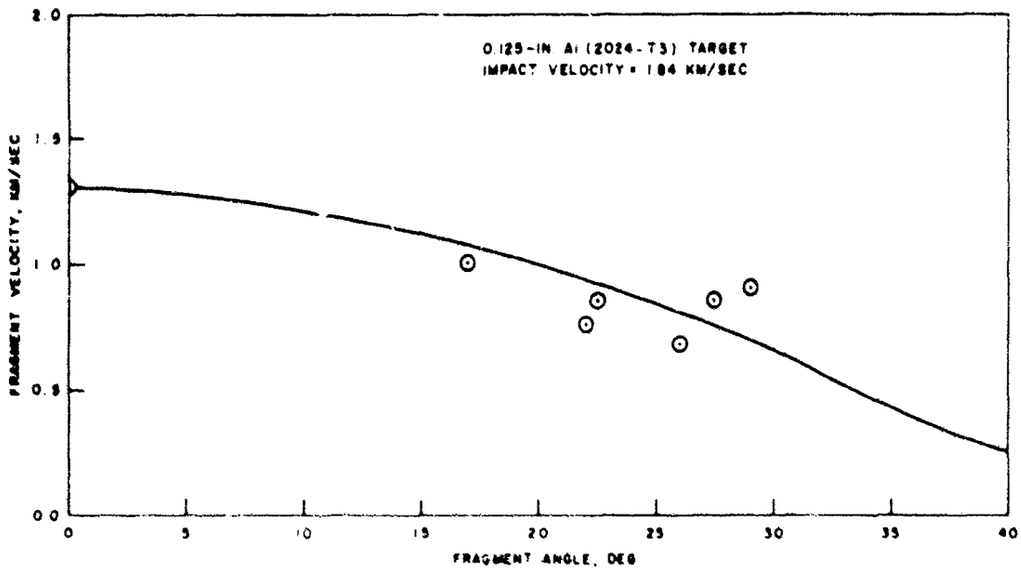

FIG. 11. Fragment Velocity Against Angle of Motion.

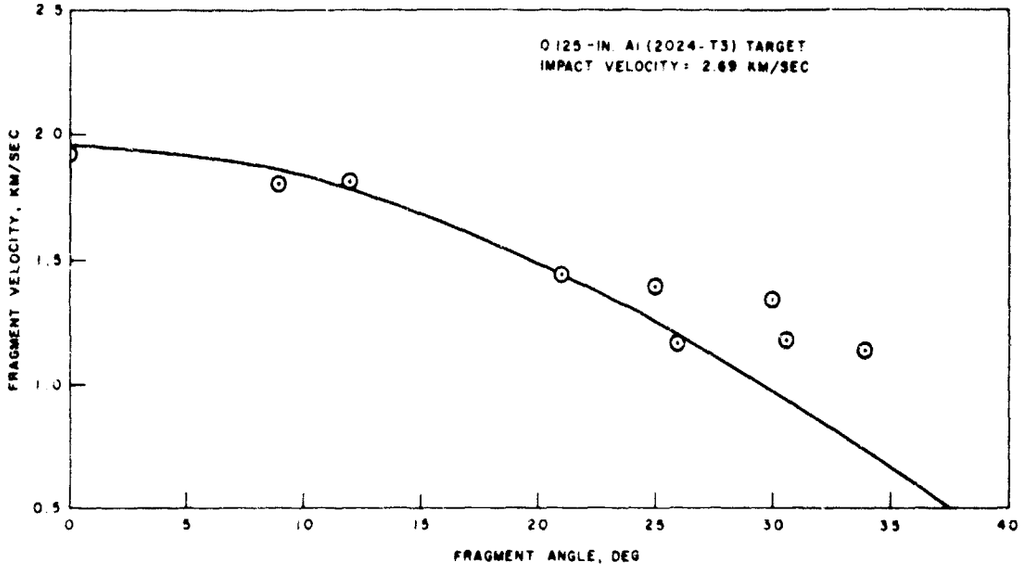

FIG. 12. Fragment Velocity Against Angle of Motion.

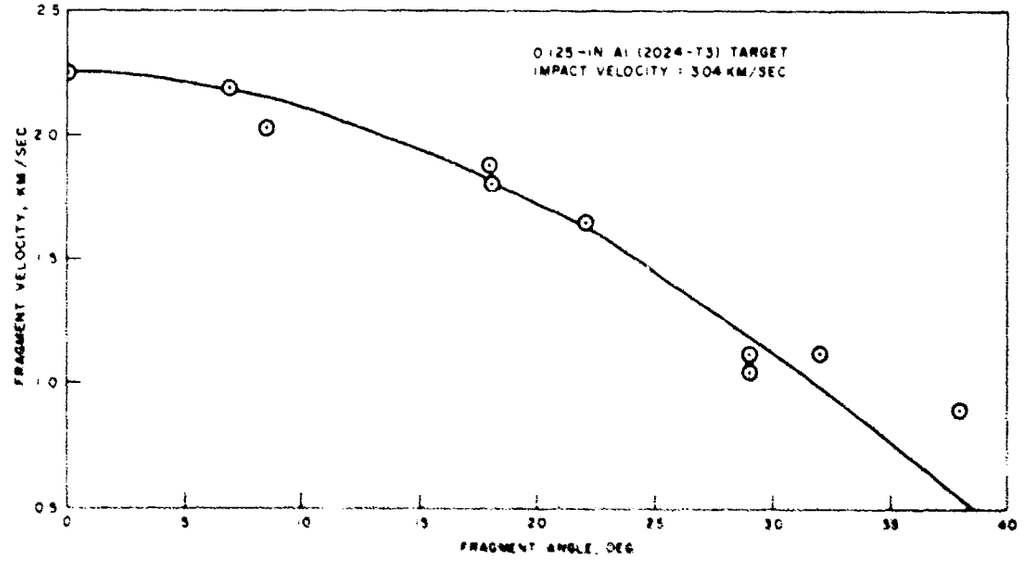

FIG. 13. Fragment Velocity Against Angle of Motion.

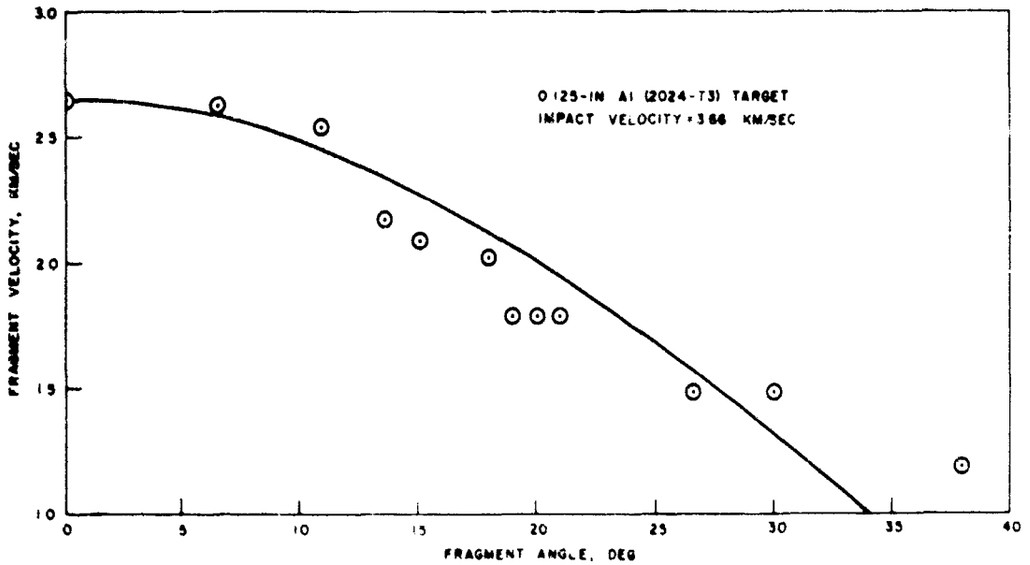

FIG. 14. Fragment Velocity Against Angle of Motion.

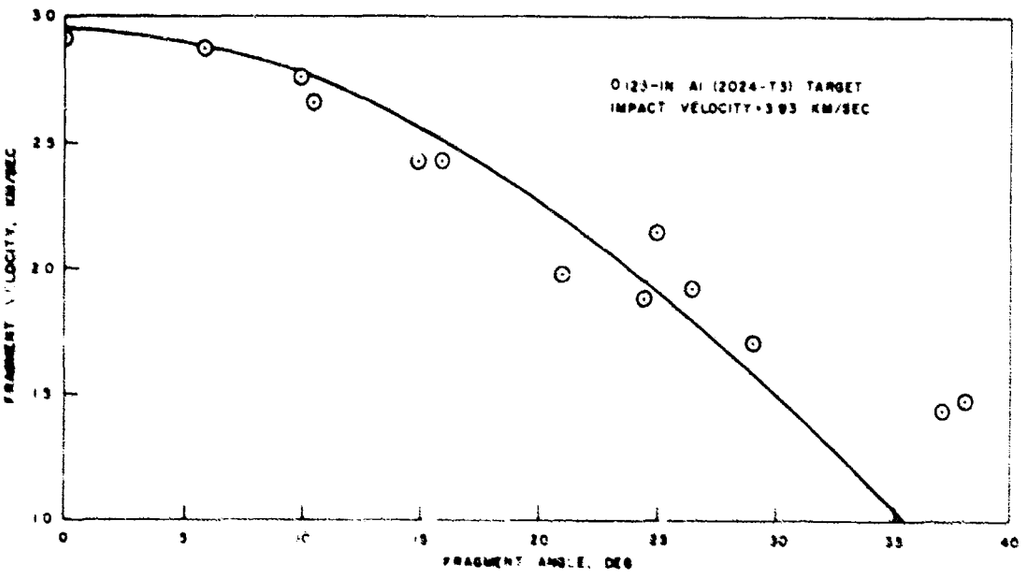

FIG. 15. Fragment Velocity Against Angle of Motion.

Hence, the residual velocity of the projectile and plug fragments will be

$$V_r = (mV_s - M_tV_t)/(m + M) \qquad (2)$$

MOMENTUM TRANSFER

In order to measure the momentum acquired by the target, a series of tests are conducted wherein the target plate is bolted to a ballistic pendulum. The results of these tests are shown in Fig. 16. Other than the 0.250-inch-thick plates, the momentum transfer is independent of the impact velocity. It first appears to depend only upon the surface area of the perforation; i.e., πDt. However, this function does not take into account the increases in perforation diameter that result from the increasing impact velocity. Hence, some relationship between this surface area and the time of perforation would seem to be more appropriate.

The experimental results with 0.125-inch-diameter spheres are particularly interesting in that they represent the largest plate-thickness-to-sphere-diameter ratio and contain the only results in which the plate is not perforated. Those tests with 0.125-inch-diameter spheres in which the impact velocity is just below the minimum perforation velocity, have the same momentum transfer to the plate as tests at double this velocity. These measurements help to rule out one reason for the drop in momentum transfer with increasing velocity that is measured with 0.250-inch plates. Because the thickness-to-diameter ratio of the 0.250-inch plate is between that of the 0.125-inch plate impacted by 0.125-inch-diameter spheres and the other plates impacted by 0.281-inch-diameter spheres, this parameter (plate-thickness-to-sphere diameter) is not believed to be the cause of the decreasing momentum transfer. No rational explanation for this variation from the behavior of the other plate-projectile systems has yet been developed.

One hypothesized effect that is not evident in these tests is target momentum due to the tiny particles coming from the impact interface. These are sprayed backward, usually at more than the impact speed, from around the periphery of the projectile. For impacts against plate targets, momentum measurements up to 40% greater than the projectile momentum are attributed to this cause (Ref. 8). The one case of excess momentum that is measured during these experiments occurs when the plate is not perforated. This single instance is not particularly significant, since it had a momentum measurement that is within the band of experimental scatter for these data.

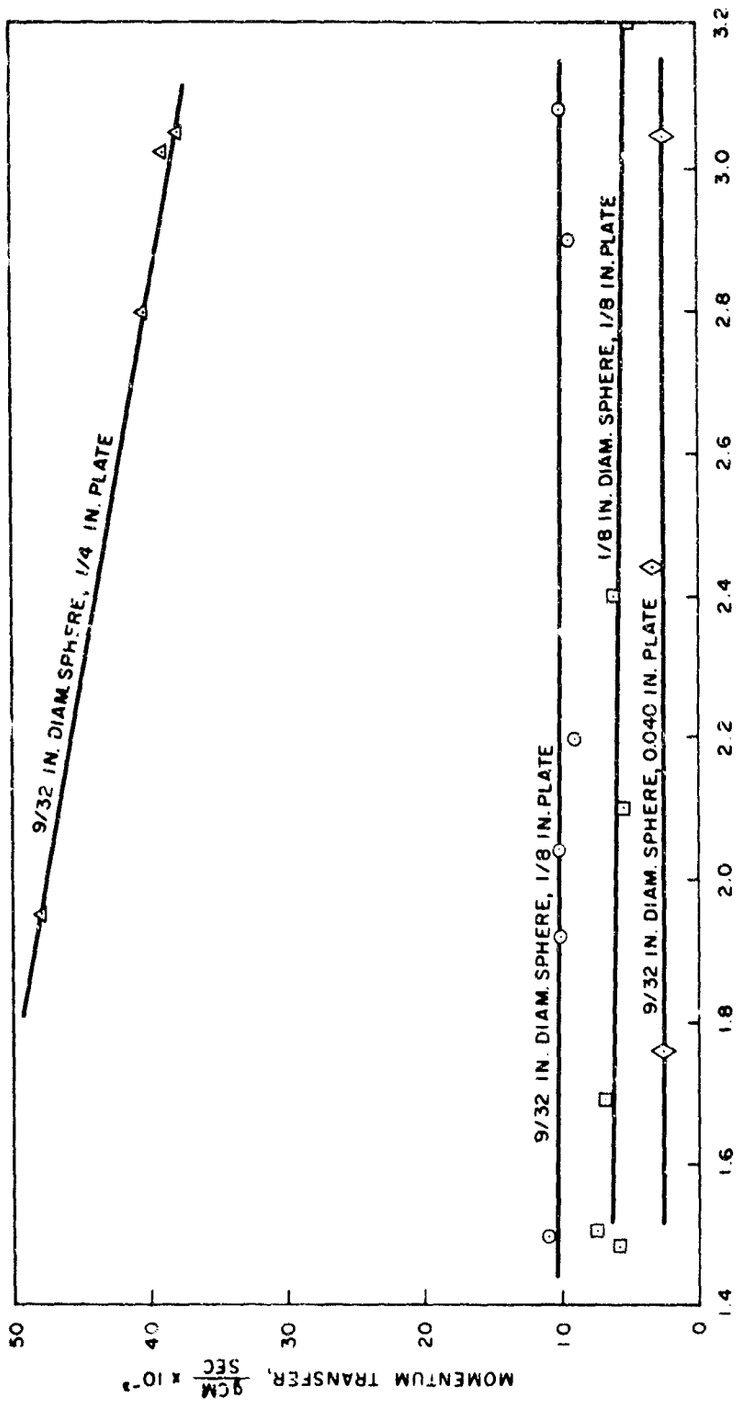

FIG. 16. Momentum Acquired by Plates During Perforation by Spheres.

CORRELATION OF ATMOSPHERIC DISTURBANCES TO FRAGMENT SYSTEM CHARACTERISTICS

ATMOSPHERIC DISTURBANCE

The disturbances associated with a particular impact system have been investigated using photographic methods and by direct measurement with transducers. Earlier work of this kind used explosively projected particles (Ref. 1-3). The Cordin camera was used with an explosive light source and a condenser lens system that revealed the shocks surrounding the fragment system (Fig. 17). Photographic records obtained in this way showed that the front of the atmospheric disturbance is at least in part the coalescence of the bow shocks from the individual particles. Direct measurements of the pressure from an impact against a plate within a chamber, which is instrumented to record the pressure in the chamber, showed that the pressures last for the greater part of a millisecond; however, the most significant variations occur within 200 or 300 μsec. The records for explosively projected particles were not very reproducible due to variations in the size and shape of the impacting particles and variations in the location of the impact with respect to the transducers.

In one series of tests, attention was concentrated on conditions at the front of the disturbance. These tests were set up to use both the Cordin camera and pressure transducers so that two forms of instrumentation could be used to check one another. Figure 18 (sample frames from the Cordin record) shows the arrival of the front at the wall in which the pressure gages are installed. Figure 19 is a sample of the transducer record for the same test. Figure 18 reveals a considerable amount of structure to the front of the shock and indicates that at least some of the high frequency variations of the transducer records (Fig. 19) are not spurious but are real variations of the pressure. An estimate of the pressure in the shock front can be obtained from the photographic data. The shock velocity is measured from the photographic data and the estimate is made by computing the pressure in the shock on the basis of plane shock theory. In order to compare this with the measurements, it is converted to the pressure of the same shock at a rigid wall. Comparison of the two forms of data is given below. These data are from a series of tests that were conducted to establish the feasibility of techniques involved.

Firing	Measured pressure	Pressure (Calculated from the shock velocity)
No. 1	40	59.1
No. 2	44	80.1

The same type of data was obtained for a chamber flushed with nitrogen. Sample frames from the photographic records are given in Fig. 20. The luminosity of the fragment field is the main difference between these records and those obtained in an air atmosphere.

FIG. 17. Eight Frames From a Cordin Camera Record Showing the Early Stages of the Impact of a Pugh Pellet Against a Thin Plate at About 3.5 km/sec.

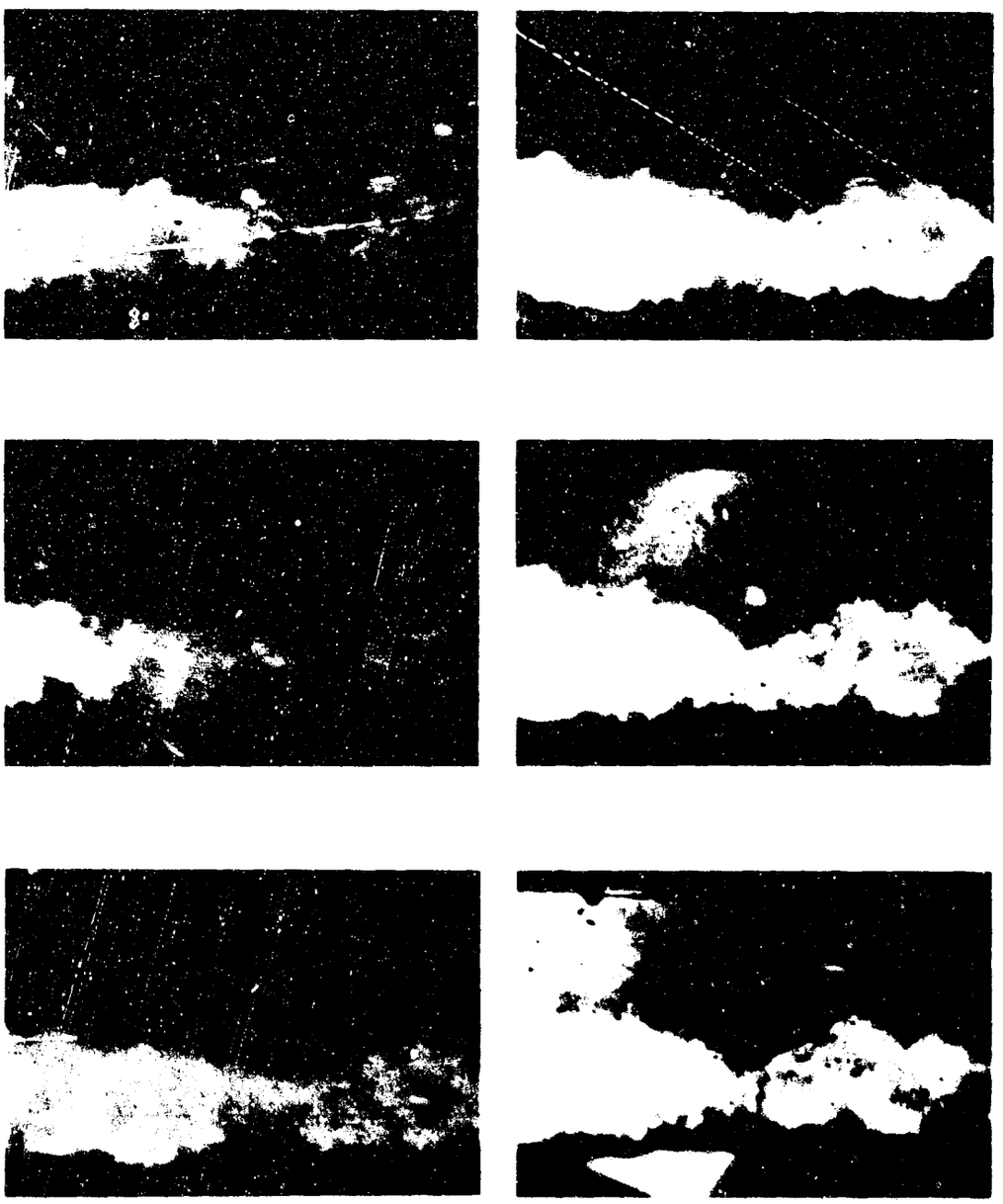

FIG. 18. Cordin Record of Shock Impingement in Air.

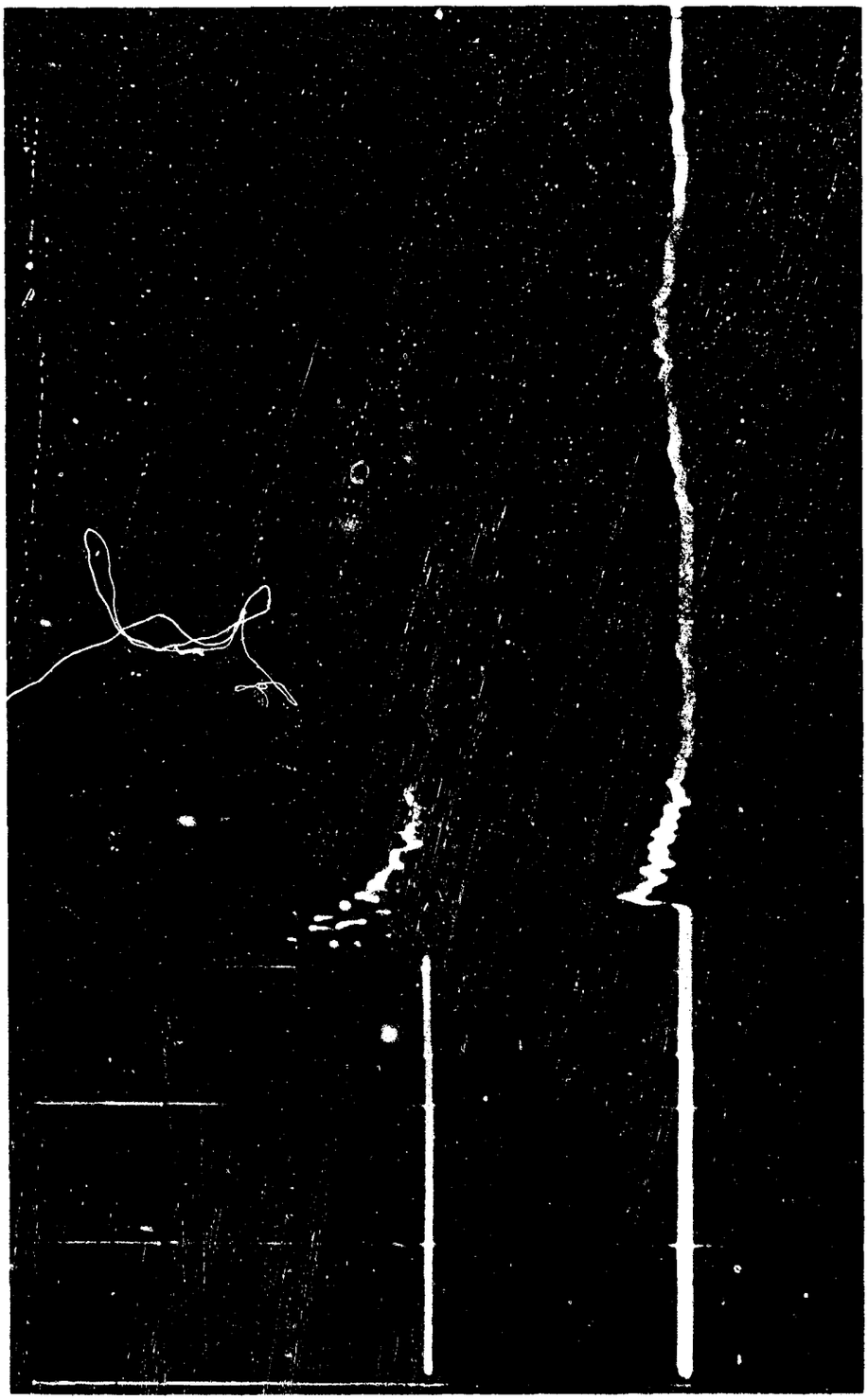

FIG. 19. Transducer Record of the Atmospheric Disturbance.

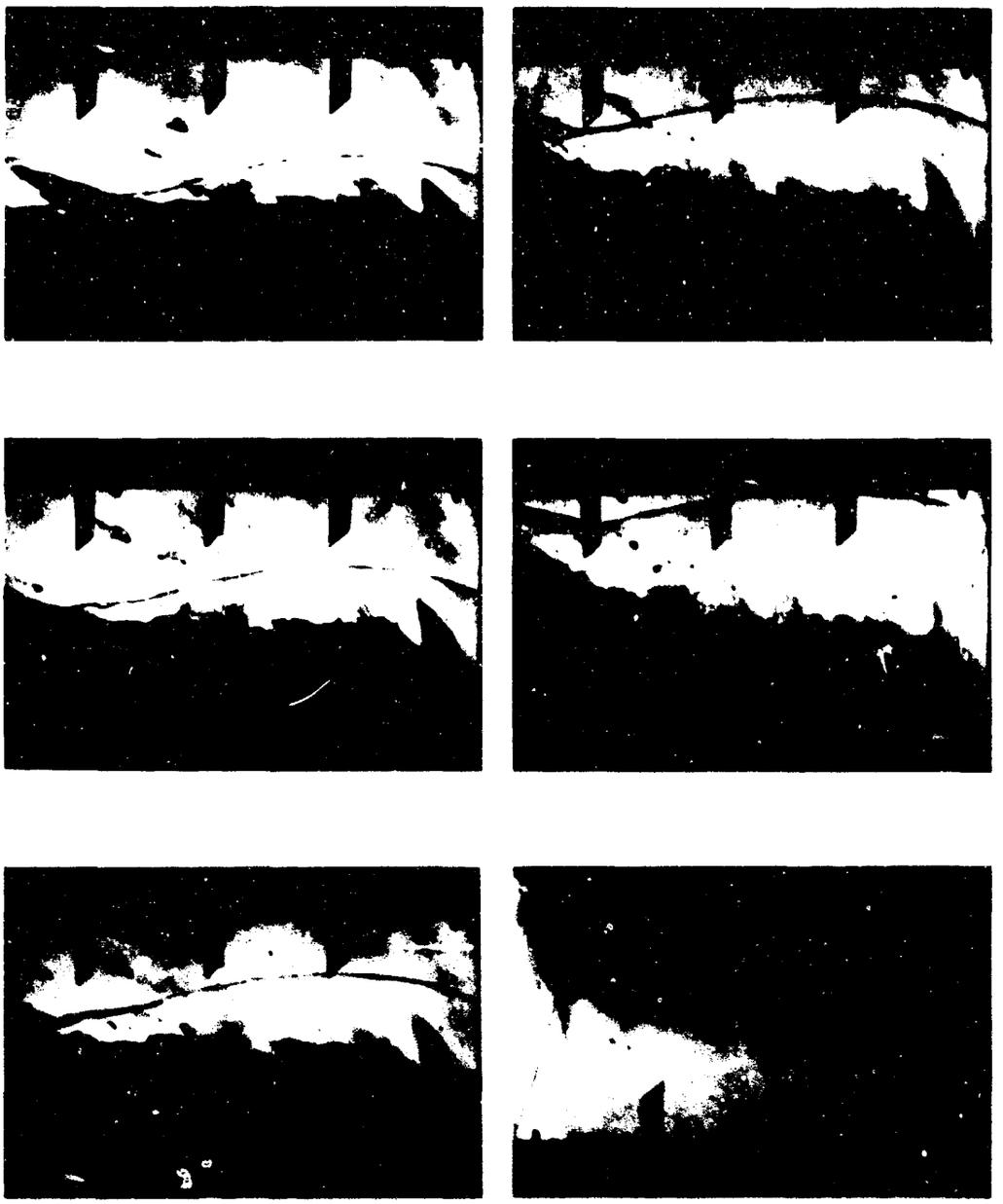

FIG. 20. Cordin Record of Shock Impingement in Nitrogen.

There are indications that the shock wave may be treated as impinging against the pressure measurement surface at normal incidence. Figure 18 shows that the part of the shock wave that contacts the gages is approximately plane. A plane wave also describes the relative times of arrival of the wave at the various gages, since this pressure pulse arrives at the three gages almost simultaneously (see the Appendix). These observations justify the use of plane shock theory in calculating the incident shock strength from the pressure records, which are measurements of the reflected shock strength. This calculation is necessary to compare the various gases used in these tests because of their varying pressure amplification factors upon reflection. These functions, calculated using standard plane shock wave theory, are shown in Fig. 21 for air and argon atmospheres. The results with a nitrogen atmosphere are practically the same as with air. In addition to the overpressure ratio, Fig. 21 illustrates that, with equal energy shocks in air and argon, the measured pressures will be within 10% of each other in the low pressure region. Thus, the anomalous pressures sometimes measured in argon atmospheres cannot be due to the differences in density, specific heat, and sonic velocity between argon and air.

Pressure Measurements for Gun-Launched Spheres

Similar tests to those conducted with explosively projected pellets were made using aluminum spheres of 2024-T6 material from a light-gas gun against the target plate on the chamber shown in Fig. 22. Velocities range between 2.3 and 4.6 km/sec. The gages used in this chamber are Atlantic Research Corporation, Model BD-15 time-of-arrival gages. In combination with charge amplifiers this circuit has a rise time of around 5 μsec. The high output of these gages reduces the noise content of the data in comparison with more sensitive blast-type gages that have also been tried. In the tests with the light-gas gun, the chamber has a plastic film forming the wall opposite the target plate. This practically eliminates any pressure effects due to secondary impacts of target and projectile fragments. It also reduces the problem of accounting for the pressure waves reflected from walls adjacent to the instrumented surface. To test the effects of various gas compositions, the chamber is flushed with air, argon, or nitrogen gas for about 5 minutes before a test. In all cases the pressure in the chamber is initially atmospheric with flow of the test gas continuing during the test.

Pressures are measured at three locations along the center line of the top surface of the chamber. Of the 32 tests in which realistic pressure-time data were obtained, 11 representative tests are assembled in the Appendix. Along with the pressure records, associated photographs of impact flash and the perforation itself are shown in most cases. The open shutter photographs of impact luminosity within the chamber serve as an indication of the amount of combustion taking place. One undesirable feature of the tests with the light-gas gun is the aluminum shear disc that frequently follows the projectile into the impact region. Accessory

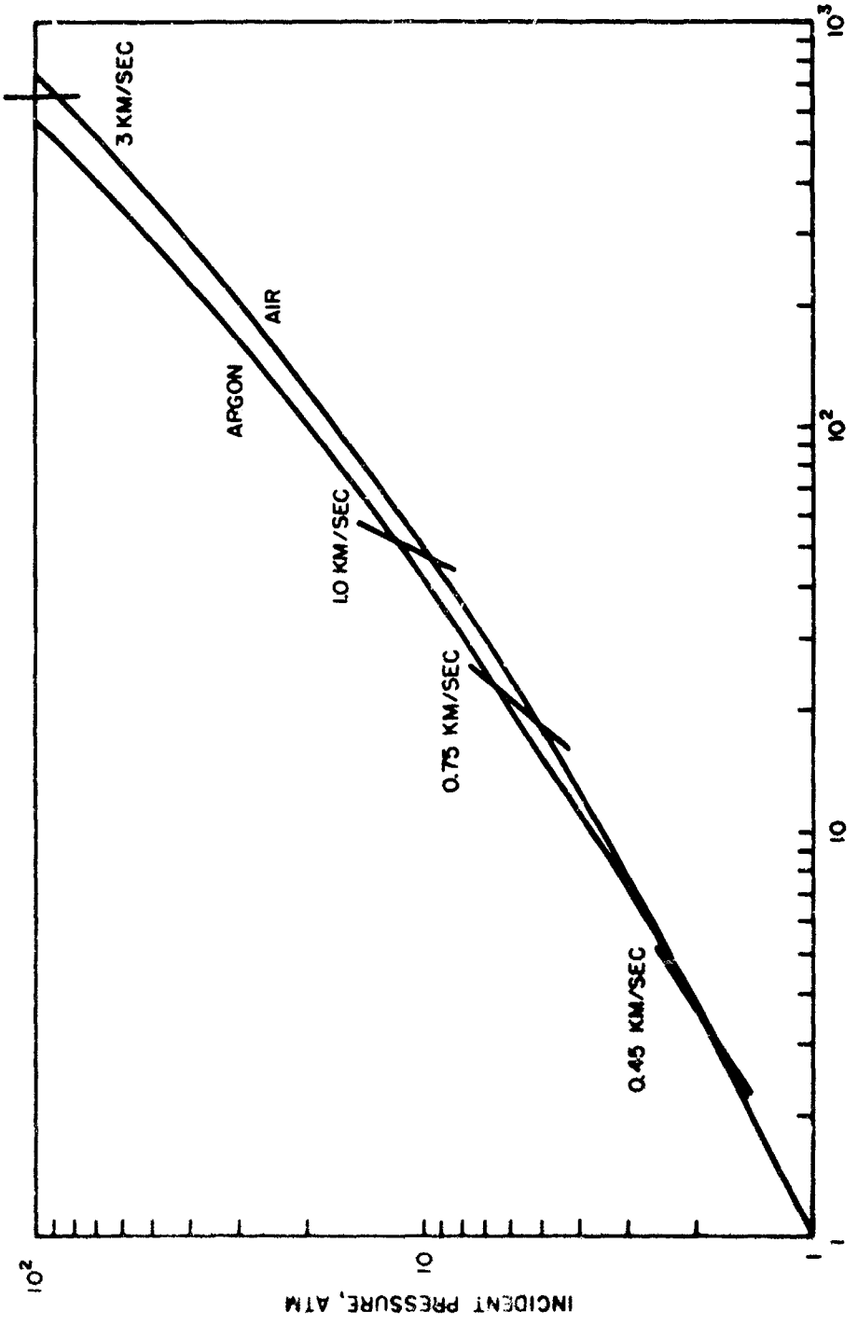

FIG. 21. Pressures Due to Plane Shocks Reflected at Normal Incidence.

impacts due to this component are apparent in several of the perforation photographs.

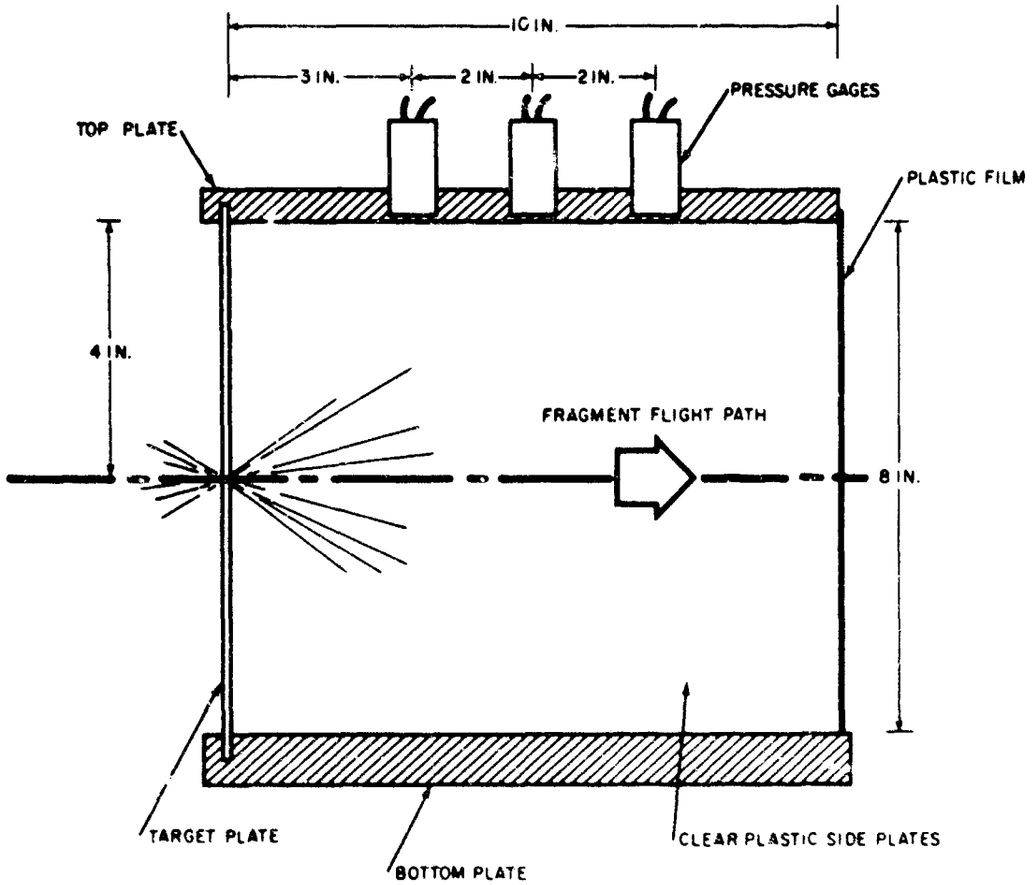

FIG. 22. Schematic Drawing of Pressure Measurement Chamber.

In general, the pressure pulse has a fairly simple pulse shape that is similar to a blast wave with an amplitude dependent upon the fragment system characteristics and with a time duration for the positive phase of 70 to 140 μsec. A second pulse frequently lags the first by roughly 300 μsec. Since the second pulse can be eliminated by removing the floor and walls of the box, it is undoubtedly caused by reflected pressure waves from these plane surfaces. Hence, the very jagged, relatively long duration pressure records commonly reported are probably the result of multiple reflections from the rigid container walls.

The peak pressures shown in Fig. 23 are calculated from the data on peak-reflected pressure of the first pulse by using the plane shock

relations shown in Fig. 21. The increase in pressure with increasing impact velocity of the sphere is proportional to between the second and third power of velocity for the plate thicknesses shown. The peak pressures also increase with decreasing plate thickness, at least to some thickness less than those tested here (t/d = 0.15). There was one test conducted in which a sphere was fired through the chamber without impacting anything except a foil switch and it resulted in a pressure below that of all but the thickest plates (t/d = 0.89). Peak pressures in air, which would support combustion, are not noticeably different from the pressures measured in argon and nitrogen that are inert. However, the still photographs do show a large amount of luminosity accompanying impacts in air in comparison with impacts in the inert gases.

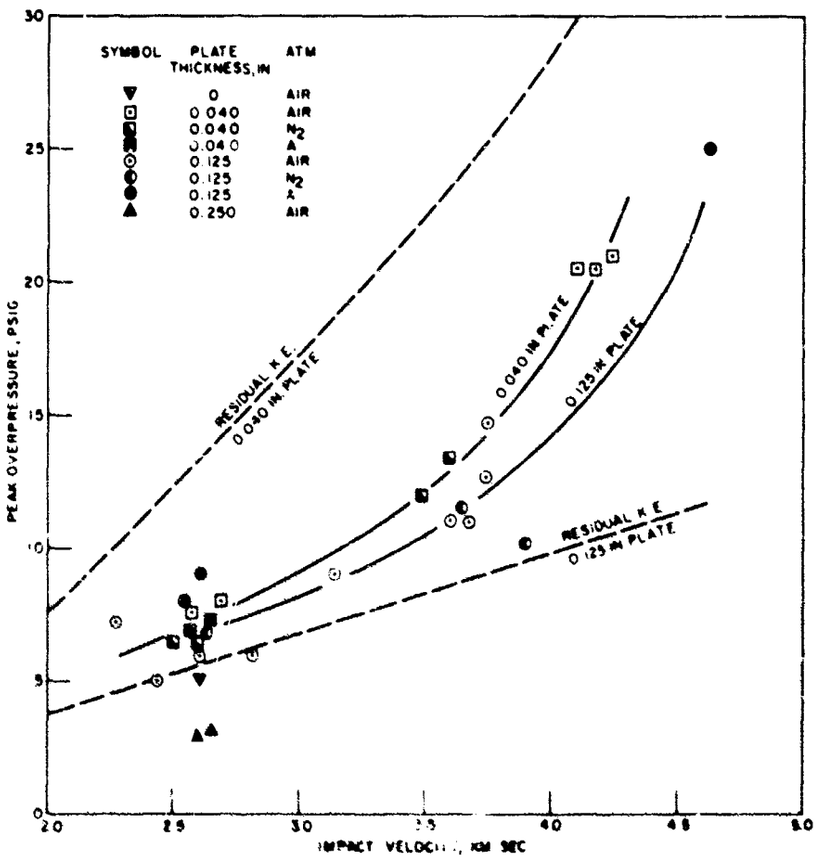

FIG. 23. Overpressure in Shock Waves at the Chamber Wall.

Information from the photographic coverage of the post-perforation events can also be used to estimate the pressure of the atmospheric disturbances accompanying perforation. A technique of backlighting, similar to that employed with the Cordin camera, is used with the six-frame Kerr cell camera to reveal the shocks and other major changes of atmospheric density. By this means, data are collected on the propagation rate of the shock surrounding the fragment system as a function of the impact velocity and plate thickness. The measurement of the propagation rates are performed near the plate to avoid as much as possible the problems of determining the propagation of disturbances near fragment wakes. Tests are also conducted in which there is no target so that an indication can be obtained of the amount of increase in pressure due to the process of perforation itself. For all tests the rates are determined at a common distance of 6 cm from the line of flight of the sphere. The data on propagation rates are presented in Fig. 24.

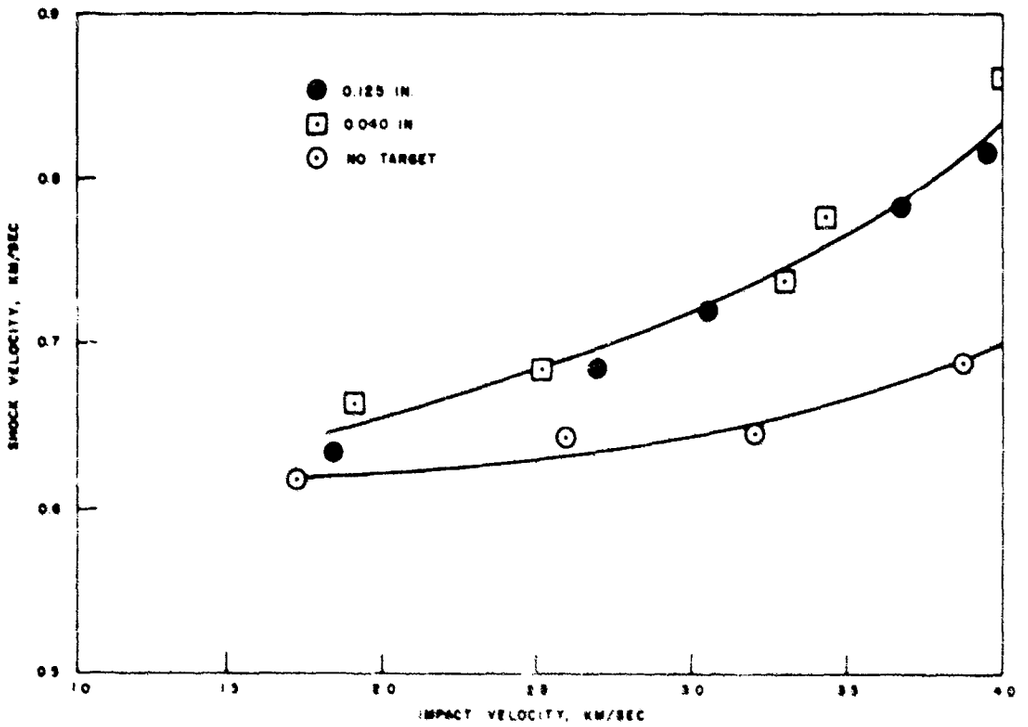

FIG. 24. Shock Velocity Against Impact Velocity for no Target and for two Plate Thicknesses.

Pressures corresponding to these propagation rates are shown in Fig. 25. These are calculated using plane shock theory that is justified as an approximation in an earlier section of this report. These data show that there are significant pressures generated near the perforations and that the propagation rates and pressures for perforated plates are significantly higher than for the bow wave of the projectile itself. The propagation rates are increased by as much as 20% and this corresponds to an increase in pressure of 76%. It is also interesting to note that there is little difference between the 0.040- and 0.125-inch plates.

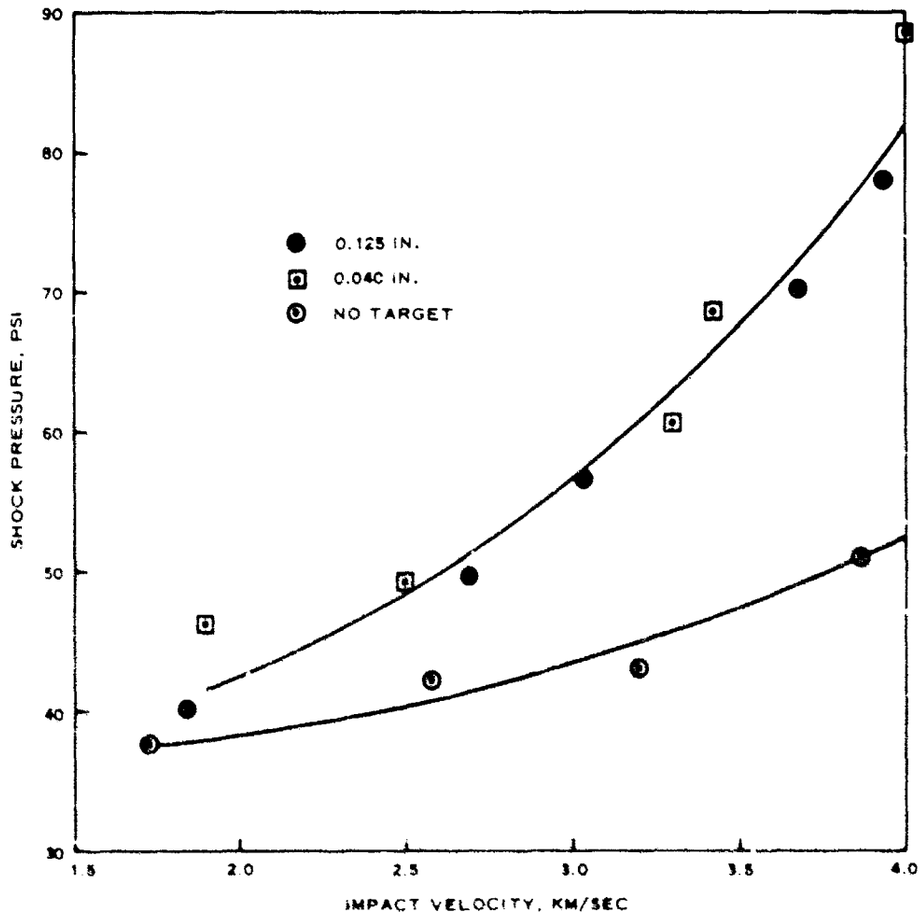

FIG. 25. Shock Pressures Against Impact Velocity for no Target and for two Plate Thicknesses.

COMPARISONS OF MEASUREMENTS TO THEORIES OF DISTURBANCE

Attempts to explain the measured pressure pulses can generally be classified into three groups. Firstly, there are explanations that postulate some mechanism of direct transfer of kinetic energy; secondly, there are explanations that postulate a significant contribution to the atmospheric disturbances from chemical reaction of the fragments with the atmosphere; and thirdly, there are explanations that postulate the generation of pressures in the surrounding atmosphere as the result of the mechanical interaction of the particle with the atmosphere. Information on which of these types of explanation is the most realistic can be obtained from studies of the fragments recovered following high-speed perforations. In the following, the main ideas of the three groups of explanations will be presented and then the conclusions from each of these will be compared to general observations on post-perforation events, experimental findings on the pressures of the disturbances, and the predicted effects on the fragment system.

Direct Mechanical Effects

Direct mechanical transfer of momentum to the pressure gages by small fragments or by vapors is obviously a possibility but it is ruled out by almost every observation. The simultaneous photographic observations and pressure measurements for the explosively projected particles show that the pressure measurements coincide with the arrival of the shock in the atmosphere. The photographic observations with the Kerr cell camera indicate a distribution of fragments for which impacts against the gages would be very unlikely events. This agrees with the further observation that the gages are infrequently hit by fragments and when this does occur the pressure records are greatly disturbed at the impact and the readings are unreliable after the impact. It is possible that vaporization might occur although there is not evidence of the condensation of vapors on any part of the equipment. However, within an inch of the perforation on the impact side of the plate there are often radial splashes of a light-gray material but this appears to be Al_2O_3. Hence, it seems quite unlikely that direct mechanical effects contribute to the measured pressures.

Combustion Processes

The heat of combustion derived from a gram of aluminum is equivalent to the total kinetic energy of this same mass traveling at 7.8 km/sec, and thus the burning of aluminum is potentially a source of a large amount of energy. It is interesting that with this large source of energy available the pressure measurements of the present work do not show any significant contribution from combustion. The flash-accompanying impact in an oxidizing atmosphere makes it clear that combustion does occur. All of these facts make it essential to take a close look at the combustion processes in order to find the reasons for the small contribution that is observed in the present work.

The following is primarily concerned with vapor-phase-combustion processes, since these appear the most likely to occur at the rates required for the present phenomenon. These processes are not well understood but two idealized models are available to describe vapor-phase combustion of either a particle at rest in a high-temperature atmosphere or of a particle in very high-speed motion with respect to the surrounding atmosphere. The main assumptions for these two models can be compared with respect to three points, (1) the source of heat for the vaporization, (2) the method of mixing the vaporized material with the combustible part of the atmosphere, and (3) the distribution of the heat generated by the combustion.

For the particle at rest with respect to a heated atmosphere the heat for the vaporization of the material is provided by the combustion process itself. The vapors and the atmosphere are mixed by diffusion. The heat generated is put into the atmosphere in the immediate vicinity of the particle and at least part of the heat returns to the particle.

For the particle in rapid motion with respect to the atmosphere the heat for vaporization is provided by aerodynamic heating of the high-speed flow around the particle. The vaporized material is removed and mixed with atmosphere by the high-speed flow. The heat generated by the combustion is released to the atmosphere in the wake of the particle and does not return to the particle.

Reaction With Nitrogen. The possibility of the molten aluminum reacting with nitrogen has also been suggested. This less energetic reaction is tested for by mounting an aluminum plate in a chamber filled with nitrogen gas at a few pounds per square inch above atmospheric pressure. The chamber is sealed after the entrance of the projectile by the impact of sabot upon a sabot stopper. This copper sabot stopper then craters providing a gas-tight seal for the central hole through which the projectile has passed. After impact at 3.2 km/sec, chemical tests of the contents of this chamber show no evidence of aluminum nitride.

Particle in a High-Speed Flow. A model of combustion processes for the particle in a high-speed flow should take into account the change in mechanical strength of the material when it reaches the melting point, since the high-speed flow will subject the body to intense forces. For this reason it is convenient to discuss the model in terms of two phases. In the first phase the particle is aerodynamically heated, and melting occurs at the surface. The molten layer is capable of flowing and is removed by the surface forces that are generated by the high-speed flow. The separation of these droplets is the start of the second phase in which the droplets are free bodies that are heated by the high-speed flow around them. This heating may be sufficient to vaporize the droplets. In this case the two phases involve similar physical processes but the size and condition of the particle is different. If, on the other hand, vaporization does not occur until the droplet is at rest with respect to the surrounding atmosphere, which is at a high temperature due to the flow

conditions, then the second phase is better described by the model of combustion for particle at rest in a hot atmosphere.

Nonreactive Melting Model. For the first phase, a simple calculation can be made of the material that will be ablated from a particle by melting from aerodynamic heating. This calculation is merely an energy balance between the incident energy flux and the thermal energy required to melt aluminum. The incident energy flux will be the product of the pressure (assumed to be hydrodynamic) and the velocity of the particle.

$$q_i = (\rho_g V^3/2)$$

The energy removed from the body in the form of heat in the ablated material is

$$q_m = m(C_p T + h_f)$$

Therefore

$$\dot{m} = C_H \rho_g V^3/2(C_p T + h_f)$$

$$dm = [C_H \rho_g V^2/2(C_p T + h_f)]ds$$

The ablated mass per unit distance may be obtained by including the velocity decay caused by aerodynamic drag.

$$dm = \frac{\rho_g V_o^2 C_H}{2(C_p T + h_f)} \int_o^s \exp(-\rho_g C_D A_s/M)ds$$

The effective heating rate across the body is roughly the integrated product of the stagnation point heating rate and the cosine of the angle between the particle velocity vector and the normal to the surface. By using this correction the mass fraction loss from the particle will be

$$\frac{m}{m} = \frac{C_H V_o^2 [1-\exp(-3\rho_g C_D \Delta s/2\rho_p d)]}{3 C_D(C_p T + h_f)}$$

Figure 26 shows this mass fraction loss for spherical aluminum particles at standard atmospheric conditions. The spheres are assumed to be initially at room temperature with a velocity of 3.1 km/sec.

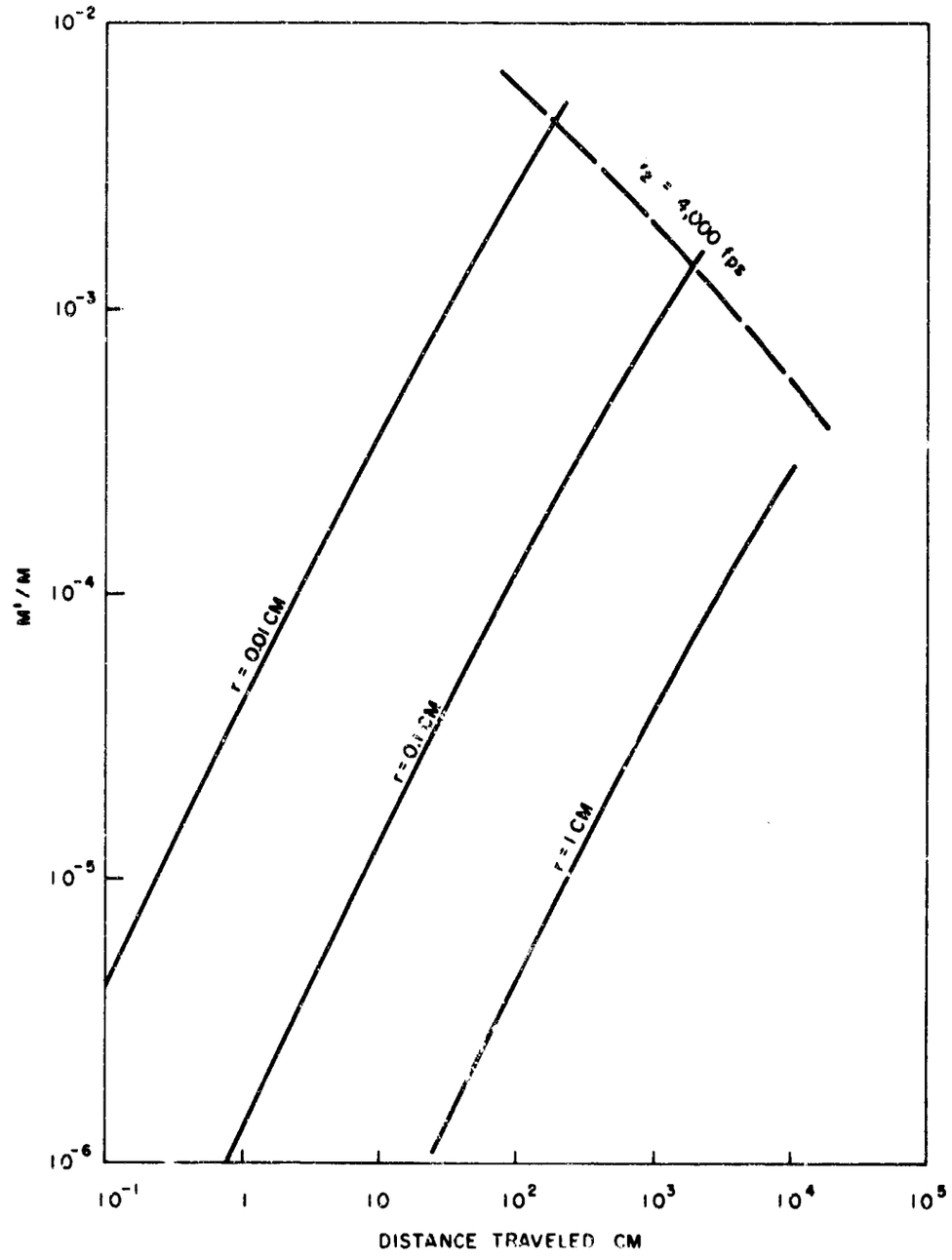

FIG. 26. Mass Fraction Loss of Aluminum Spheres due to Melting Ablation in an Air Atmosphere: V_∞ = 3.28 km/sec.

In the second phase, steady-droplet configuration requires that the surface tension of the droplets must be greater than the forces tending to remove more material from the droplet. This is equivalent to a requirement that there be a maximum stable droplet size for the given velocity of flow. Below this maximum size the losses of mass are by vaporization and applying the same arguments to the ablation by vaporization that is used for ablation by melting one finds that

$$\frac{m'}{m} = \frac{C_H^1 V_o^2 [1-\exp(-3\rho_g C_D \Delta s/2\rho_p d)]}{3 C_D (C_p T + h_v)}$$

for Δs the distance travelled by the droplet with respect to the moving atmosphere. Clearly, the first phase of the process is the controlling one with respect to the determination of the maximum contribution by combustion according to this model. The equations above are only able to determine the extent and rate at which the melted material can enter the final combustion process.

One factor that would tend to increase the rate of ablation of droplets from the fragments would be the surface roughness of the impact fragments. Another is the possibility of a higher initial temperature of fragments coming from the zone near the impact interface (Ref. 9). Similarly, factors such as rotation of the fragments and inhibition of ablation by a layer of aluminum oxide (which has a higher melting temperature than aluminum) would tend to decrease the ablation rate. In either case, it seems unlikely that particles larger than 50 microns in diameter will lose any appreciable portion of their mass. At most, only a few percent by weight of the particles recovered beyond thin plate impacts are less than 50 microns; consequently nonreactive, melting ablation does not appear to be a likely mode for rapid energy release.

Particle at Rest in Hot Atmosphere. The combustion of particles in a hot atmosphere has recently been the subject of a large amount of effort in connection with the steady-state combustion of aluminum in gas burner flames (Ref. 10-12). From these studies, along with the rigid constraints placed upon aluminum combustion by thermodynamic considerations, a description of particle burning has emerged. The model described here is basically that proposed by Brzustowski and Glassman (Ref. 13).

After ignition and the attainment of steady-state conditions, the vaporizing aluminum droplet is surrounded at some distance by a combustion zone. The reaction rate and the distance of the combustion zone from the body are controlled by the transport of aluminum vapors from the particle and oxygen from the atmosphere into this zone. Probably the first product oxide that forms is AlO, a vaporous oxide species that only exists at temperatures above the boiling point of alumina. However, the heat of vaporization of Al_2O_3 is greater than the heat of combustion of aluminum

(Ref. 14). Consequently, there is insufficient heat to sustain all of the AlO and it condenses within the reaction zone into submicron sized Al_2O_3 droplets. This condensation maintains the reaction zone temperature at the boiling point of alumina, 3800°K. At this stage in the reaction, external sources such as aerodynamic heating of the particle are small in comparison with the heating from the reaction zone. The principal modes of heat transfer to the particle from the reaction zone are radiation and the conduction resulting from liquid alumina condensing on the cooler molten aluminum surface.

Consider the effect of placing this burning particle in a hypersonic air stream. There will be a high-pressure, high-temperature cap composed of the constituents of both the ambient atmosphere and the vaporizing particle. Extreme conditions in this gas cap will be located at the stagnation point at which, at the higher velocities, dissociation might also occur. In comparison with ambient atmospheric conditions, the greater partial pressure of oxygen in the gas cap will shift the reaction zone closer to the particle. This results in an increased heating rate on the body and a corresponding increase in the ablation rate of the particle. Ionization of the atmospheric gases would amplify these effects. Hence, the combustion of impact fragments should be more energetic than the reaction of particles ignited in burner flames. It will be shown that the burning times of impact fragments are reduced by an order of magnitude over comparable sized fragments ignited in a flame.

Tests in which fragments are captured in paraffin after passing through 5 inches of air net all types of oxides other than the flakes and do capture some aluminum that are partially molten. When this apparatus is evacuated to 0.03 mm of mercury no oxides are found but many aluminum particles are recovered that are completely or partially molten. The tests in which fragments are collected in pans result in aluminum, ceramic solids, and flake-type oxides. These oxide particle descriptions and the pressures and O_2 partial pressures under which they are formed are quite similar to the observations of Mellor and Glassman who studied the combustion of aluminum wires in an O_2-CO_2 atmosphere (Ref. 15).

Mechanical Interactions With Atmosphere

The aerodynamic pressures acting on high velocity fragments result in a drag force and loss of kinetic energy with time. At supersonic velocities these pressures result in nonisentropic shock waves. The kinetic energy losses of the body are largely dissipated in the shock waves; hence, the pressure ratio across the shock depends upon the rate of kinetic energy loss of the body. For a relatively smooth body this energy loss can be shown to be proportional to $V_o^2 \exp(K\Delta s/d)$ where Δs is the distance traversed and d is a characteristic body dimension. The rate of kinetic energy lost per unit distance traversed is directly proportional to the initial velocity squared and inversely proportional to the body dimension. Small bodies thus lose energy more rapidly and in a more confined space than larger bodies. In terms of the fragment system this

means that close to the plate the smaller particles will lose more energy per unit mass than larger particles. With respect to these energy losses as a function of the fragment system characteristics, recall that higher impact velocities and thinner target plates result in both finer particle sizes and greater post-perforation velocities.

There is one other source of kinetic energy losses, which is easily forgotten, that contains quantities of energy of the same order of magnitude as the combustion energy. This is the kinetic energy lost with the ablated mass of the fragment system. Because the material that is ablated from the surface leaves either in the form of vapor or relatively tiny droplets, it essentially releases any kinetic energy it has immediately upon departure. Again, high velocity and small particle sizes favor these losses. Consequently, due to the fragment-size distribution and the initial residual velocity, thin plates and high impact velocities should result in the most rapid energy transfer.

These same variables, impact velocity and plate thicknesses, affect the measured pressures in a manner qualitatively similar to that predicted on the basis of kinetic energy losses. An estimate of the initial post-perforation kinetic energy of the impact system is calculated from the data in Fig. 2, using Eq. 2. This energy is plotted in Fig. 23 to a scale appropriate for comparison with the peak shock wave pressures. On the basis of fragment system characteristics, the increasing pressure with increasing velocity and the greater pressures behind thin plates are expected features of this system. Although this kinetic energy has these qualitative features of the shock wave pressures, the difference in pressures with plate thickness is much smaller than would be expected from simple energy considerations. In fact, based upon our neglect of the differences in particle sizes with these plates, one might expect the difference in pressures to be even greater than predicted. There are several possible explanations of these discrepancies.

These quantitative differences between the pressure records and the relative values of the kinetic energy estimates may be caused by interactions between the particles that invalidate the superposition assumption that is implicit in the energy calculations. Another possible cause of the small difference in pressure between the 0.040 and 0.125-inch-thick plates is the three-dimensional aspect of the fragment field. With pressure measurements made such a short distance from the projectile flight path, only the closest regions of the fragment field would be expected to contribute to the initial pressure pulse. High-speed photographs of perforations show that at the same velocity, a thick plate may tend to have the larger particles distributed along the surface of the fragment cone envelope while thin plates have the fragment mass concentrated at the front of this cone (Ref. 4).

ADDITIONAL EXPERIMENTAL RESULTS

Ignition. A few tests were conducted in an attempt to obtain photographic indications of the amount of material that is ablated from aluminum spheres. The intent was to compare the trails of spheres launched from the light-gas gun with the trails of explosively projected particles. The indications are that the spheres ablated far less than the particles. Collateral streak-camera measurements bear this out.

It may be that the gun-launched spheres are indeed ablating less due to the fact that these projectiles have a well-established aluminum oxide coating while the freshly formed particle from the explosive projector presents a clean aluminum surface. Alumina has a higher melting temperature and greater specific heat than aluminum and the alumina layer may have suppressed the surface melting. To test this hypothesis, spheres are cleaned by an amalgamation process using alcoholic mercuric chloride and then are mounted in sealed sabots to preserve an oxide-free surface. This whole procedure is conducted in an inert atmosphere to preserve the surface. One sphere that had been treated in this way and then fired at 3.3 km/sec produced a small source of luminosity without any indication of luminosity in the wake of the sphere. Apparently, the surface was reactive but there was no indication of enhanced ablation. One other factor that effects ignition and combustion rates is the density of fragments. This effect is due to principally radiative heat transfer between particles. In burner flames, ignition of one particle appears to trigger the ignition of others (Ref. 12, pp. 21 and 22).

Luminosity. The principal evidence for the existence of combustion of aluminum impact fragments in an oxidizing atmosphere is the brilliant flash following the passing of particles as they traverse the first meter or less beyond the target. High-speed photographs of the impact fragments in this region frequently show a stream of material trailing from a corner of the larger fragments and a cone of material following tiny fragments. This material is, sometimes, initially opaque with luminosity occurring some distance behind the particle, while other particles show the entire stream as luminous. This material appears to be micron-sized aluminum droplets ablated from the fragment surface (Ref. 16). It has been reported that this luminosity is only present in aluminum pellet firings at velocities greater than 3 km/sec (Ref. 17). In the tests reported here, luminosity beyond the target is only evident when the average velocities of the impact fragments are greater than 2.5 km/sec.

There are at least two sources for this luminosity. A plasma of vaporized aluminum generated by the extreme pressures at the impact interface is the initial source of luminosity on the impact side of the target (Ref. 18). Spectroscopically, light from this source would exhibit the characteristic lines of aluminum. The second source of luminosity, and cause of the flash beyond the target plate, is combustion of the fragments. The principal source of aluminum combustion luminosity is thermally

excited AlO (Ref. 19 and 20); consequently, AlO bands will be prominent in the spectra. Time-resolved spectroscopy indicates that the various features of the spectra of pellet luminosity in the order of their appearance are ballistic shock, atomic spectra of the pellet material, and AlO bands. The peak intensity of the AlO bands occurs 4 to 180 μsec after the ballistic shock (Ref. 18 and 21). Hence, the peak luminosity of aluminum pellets, which is due to the vapor-phase combustion of ablated material, always happens in the wake of the pellet. The brightness of the luminosity in these early pellet studies is estimated to be 30,000 lumens and is independent of the pellet velocity (Ref. 17).

The physical characteristics of the luminosity also indicate the source as being vapor-phase combustion in the wake of individual particles. Still photographs such as Fig. 27 show that most of the luminosity comes from diffuse regions with only a few sharp tracks indicating surface reactions on the fragments. The velocity of impact shown in Fig. 26 is only slightly above the minimum impact velocity at which luminosity is apparent beyond the plate. The standoff between the luminous region and the plate may be a transient space through which the fragments are being aerodynamically heated to the melting temperature. The vibrational temperature of the luminous wake is determined to be 4100°K (Ref. 21), a figure that agrees closely with the 3800°K vaporization temperature of Al_2O_3 at atmospheric pressure. The maximum duration of luminosity of an individual droplet from a pellet is approximately 100 μsec (Ref. 17 and 22). In the present tests the total flash duration is less than a millisecond. In contrast, the burning times of 35-micron aluminum particles in flames are between 1 and 30 ms (Ref. 23 and 24). This reduction in burning times for hypersonic particles can be attributed to the greater pressures in the combustion zone caused by the shock wave ahead of the droplets (Ref. 25).

Particle Collection. In order to obtain data on the occurrence of combustion, the fragments are collected in paraffin beyond the target and in trays below the path of the fragments. These recovered particles are mounted in plastic and are then polished and etched to reveal the internal structure of the particles. These mounted impact fragments are observed microscopically for indications of melting or chemical reaction. The possibility of fragment heating or deformation upon impact with the paraffin recovery medium is considered. However, at least 95% of the total number of recovered fragments show no signs of either melting or oxidizing reactions. There are also no indications of the particles reacting with the paraffin. Of those few particles that are modified, there is no indication that any larger percentage of small particles than larger particles are changed.

The oxide fragments that are collected are of three types: ceramic solids, flakes, and a coral structure. The ceramic solids have a gray to black color with a surface texture only slightly more rounded than the aluminum fragments. The X-ray diffraction indicates that these are

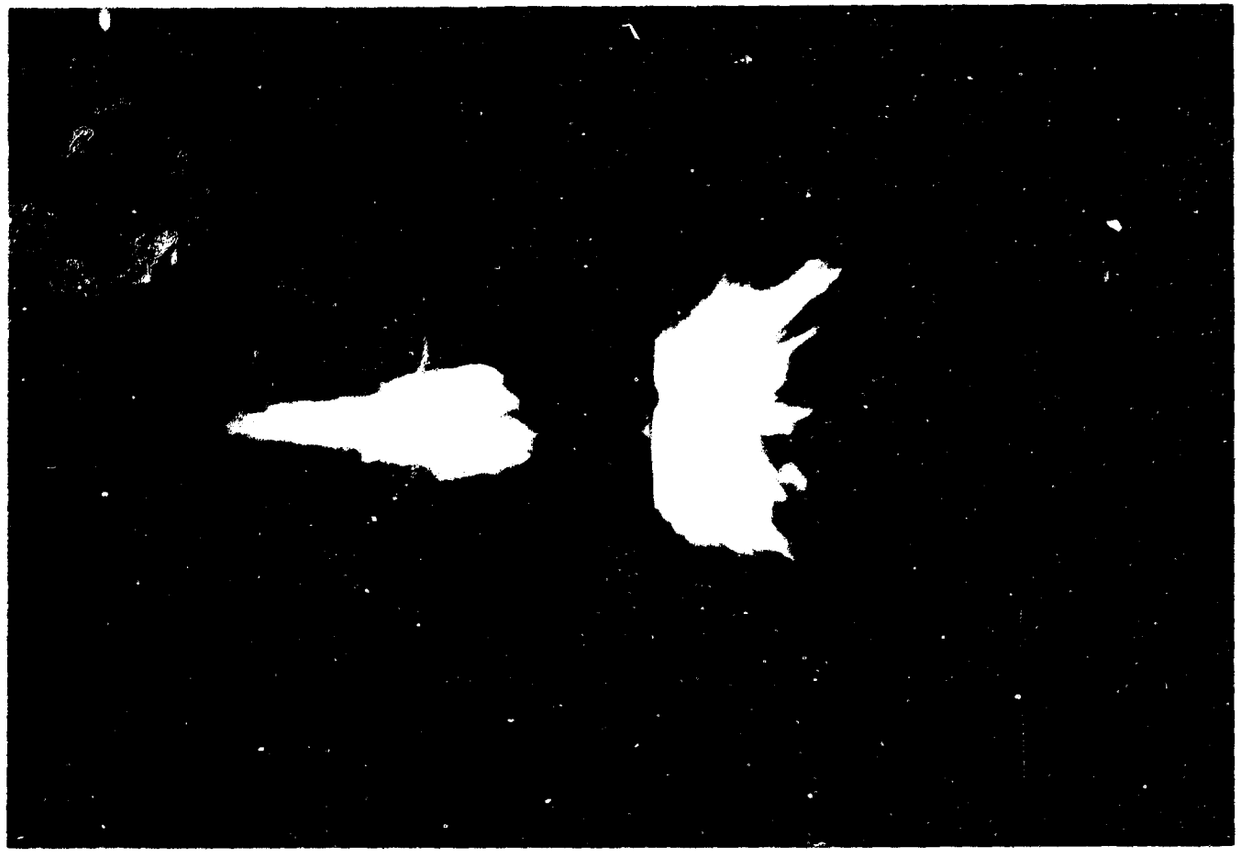

FIG. 27. Still Photograph of a Plate Perforated by a Sphere.

γ-Al_2O_3 (see Table 2). Their only internal structure consists of a few randomly distributed short surface cracks. Micro hardness tests result in the shattering of these particles. In one case, a 220-micron ceramic oxide, which had been collected in paraffin, contains perhaps a dozen aluminum inclusions of various sizes. Some of these are on the surface of the particle while others are completely immersed. The flake-type oxides are glossy black with a nodular surface texture. These are very fragile oxides that could not be effectively polished due to the surface tearing away. Flake-type oxides seem to be a collection of platelets, each of which may be an agglomeration of smaller oxide particles. The coral-structured oxides are externally gray in color and rather mossy appearing. Internally, they have a reflectivity only slightly less than aluminum with a structure consisting largely of spherical voids of a variety of sizes. The X-ray diffraction analysis of this material reveals that the sample analyzed contained aluminum plus other substances that can not be identified.

TABLE 2. X-ray Diffraction Analysis of Fragments

Aluminum		Ceramic Solid		Coral Structure	
Line	Intensity	Line	Intensity	Line[a]	Intensity
2.34	10	2.37	10	1.88	10
2.02	5	1.99	8	2.09	9
1.22	3	1.215	7	2.33	8
1.43	2	1.42	7	1.228	5
....	..	....	..	1.023	5
....	..	....	.	0.903	5

[a] Intense lines 4.25, 3.05, and 2.30 are believed to be due to the mounting clay and are eliminated.

The coral structure is the only oxide type that is ever found in intimate contact with aluminum particles; and among the specimens of this type, these are fairly common. When the coral-structured oxide is in contact with an aluminum particle a large grain structure appears in the oxide adjacent to the interface. It could be caused by that region cooling more slowly than the rest of the oxide. In addition to these oxide fragments, there is a white smoke that is often found on surfaces adjacent to impacts; this is probably the micron-sized Al_2O_3 that has been reported (Ref. 13). None of the oxidized fragments have an oxide layer surrounding an aluminum core.

In contrast with most of these oxides, aluminum fragments have quite high reflectivity. The melting zone on partially molten particles is marked by the appearance of internal voids and the disappearance of the fine-grain structured surface markings.

It may be concluded that the failure of significant pressure differences to arise as a function of the partial pressure of oxygen in the atmosphere is an indication that only a few percent of the fragmented mass are burned in air. Although 3,170 cc of air per gram of aluminum are required for combustion, lack of oxygen does not appear to be suppressing the reaction. The limiting feature upon combustion seems to be the ablation rate.

SUMMARY

The qualitative features of the deformations produced in the impact of an aluminum alloy sphere against an aluminum alloy plate are summarized pictorially in Fig. 1. The deformations of the projectile are an important factor in the dependence of the hole size on the impact velocity. At low velocity the principal failure of the perforation is clearly by plugging and the evidence from the recovery of fragments and from measurements of momentum transfer favor plugging as the principal failure mode at higher velocities. As the velocity increases above the minimum velocity for perforation other modes of failure, such as spalling and the conchoidal fractures that follow trajectories of maximum shear, contribute to the formation of a large number of fragments.

Photographic evidence indicates that the pressure disturbance accompanying the perforation is the result of the coalescence of the individual disturbances from fragment system. The ratio of the pressures in this disturbance to the pressure in the wake of the impacting projectile increases significantly as long as the fragment system maintains a high number of fragments and a high average velocity for the system.

For the case of spheres fired from a light-gas gun against aluminum alloy plates there is no significant difference observed between inert atmosphere and an atmosphere in which combustion has occurred. This is consistent with the results of a calculation of a very small rate of ablation and the conclusion that the contribution to the pressure effect by combustion processes is controlled by the rate of ablation.

Appendix

PRESSURE-TIME RECORDS, PHOTOGRAPHS OF PERFORATIONS, AND STILL PHOTOGRAPHS OF PERFORATION FLASHES

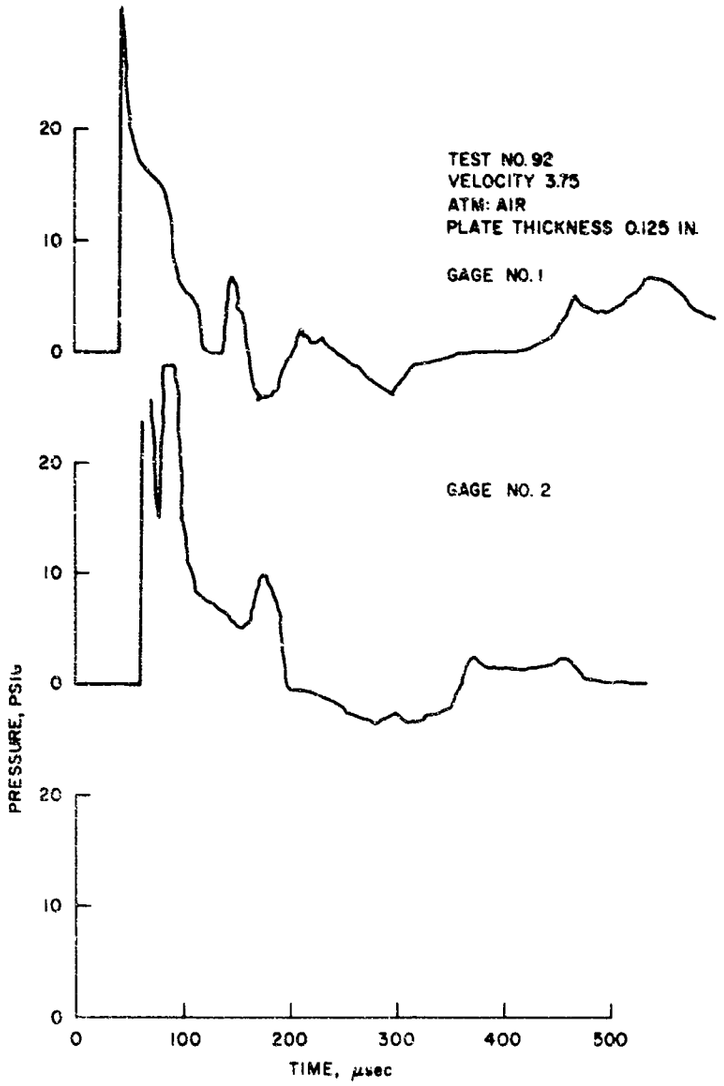
TEST NO. 92
VELOCITY 3.75
ATM: AIR
PLATE THICKNESS 0.125 IN.
GAGE NO. 1
GAGE NO. 2
PRESSURE, PSIG
TIME, μsec
20
10
0
100
200
300
400
500

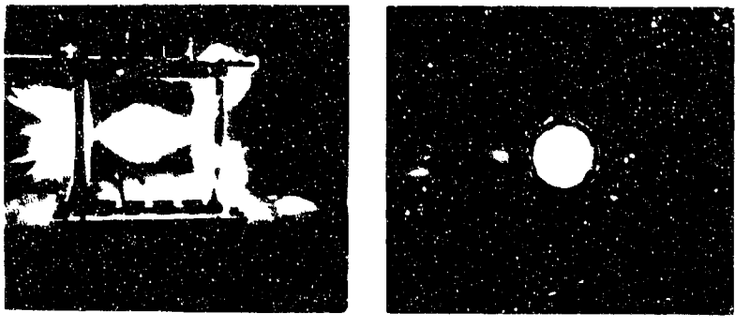

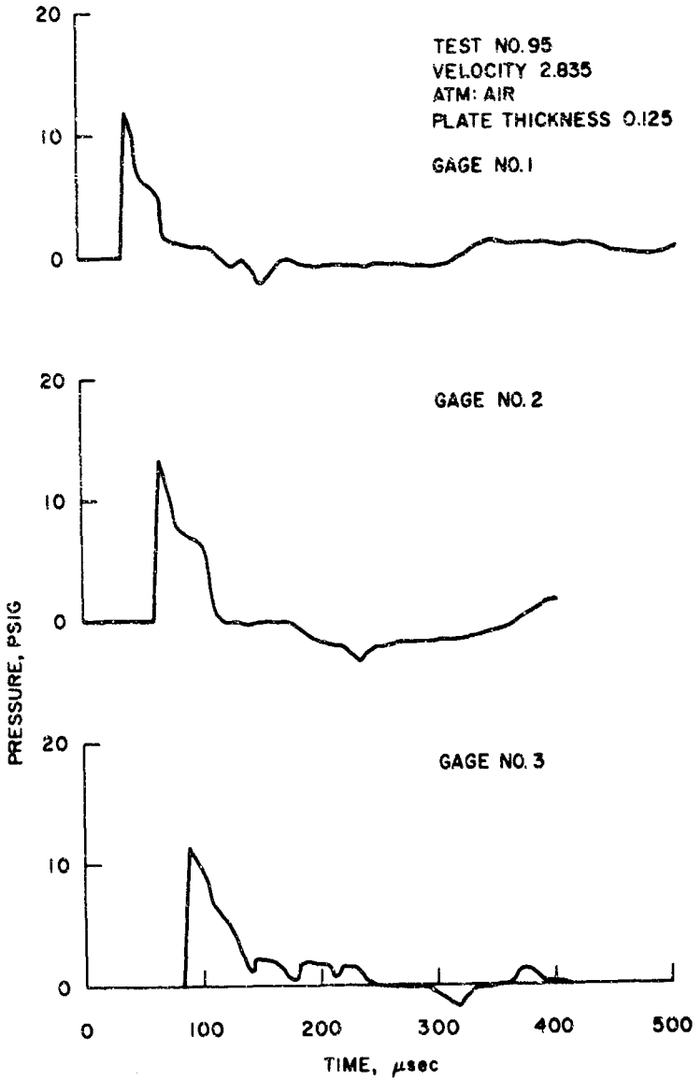
TEST NO. 95
VELOCITY 2.835
ATM: AIR
PLATE THICKNESS 0.125
GAGE NO. 1
GAGE NO. 2
GAGE NO. 3
PRESSURE, PSIG
TIME, μsec
20
10
0
100
200
300
400
500

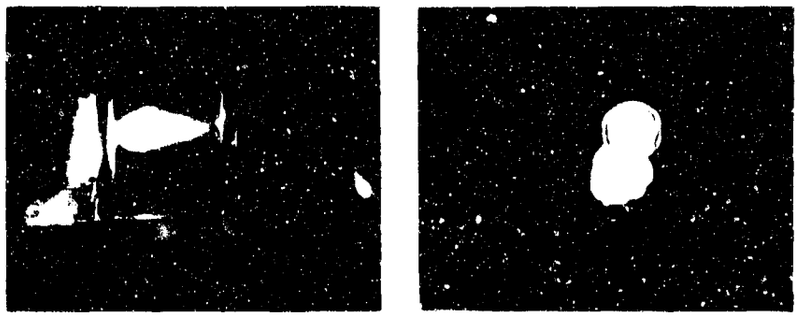

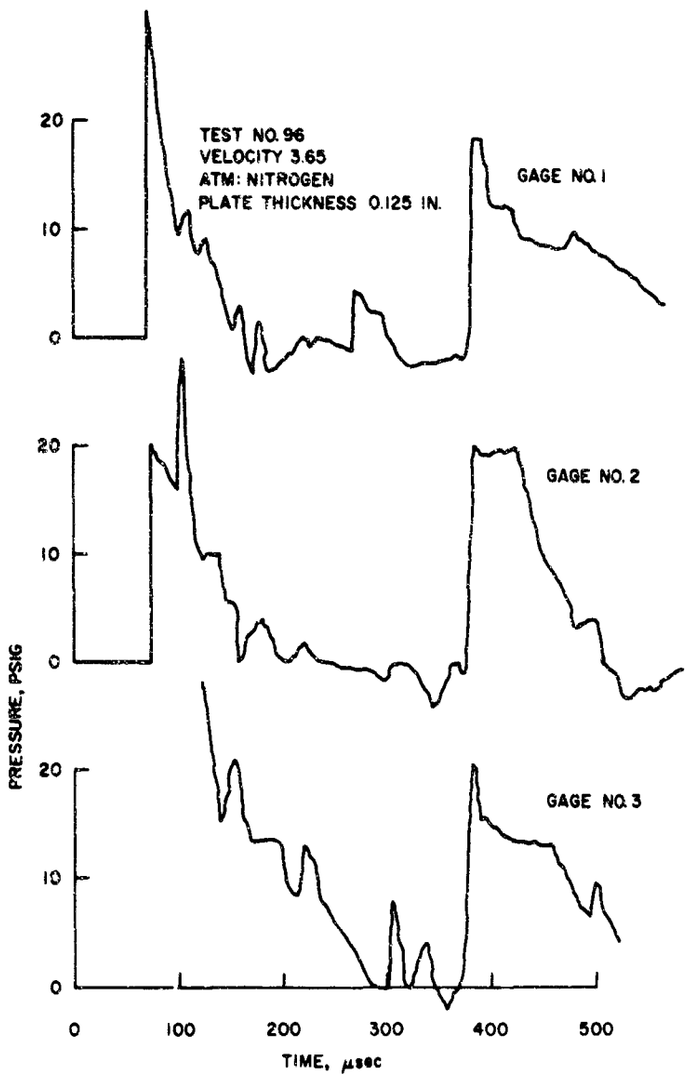
TEST NO. 96
VELOCITY 3.65
ATM: NITROGEN
PLATE THICKNESS 0.125 IN.
GAGE NO. 1
GAGE NO. 2
GAGE NO. 3
PRESSURE, PSIG
TIME, μsec
0
10
20
100
200
300
400
500

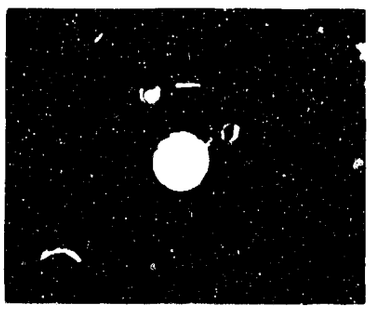

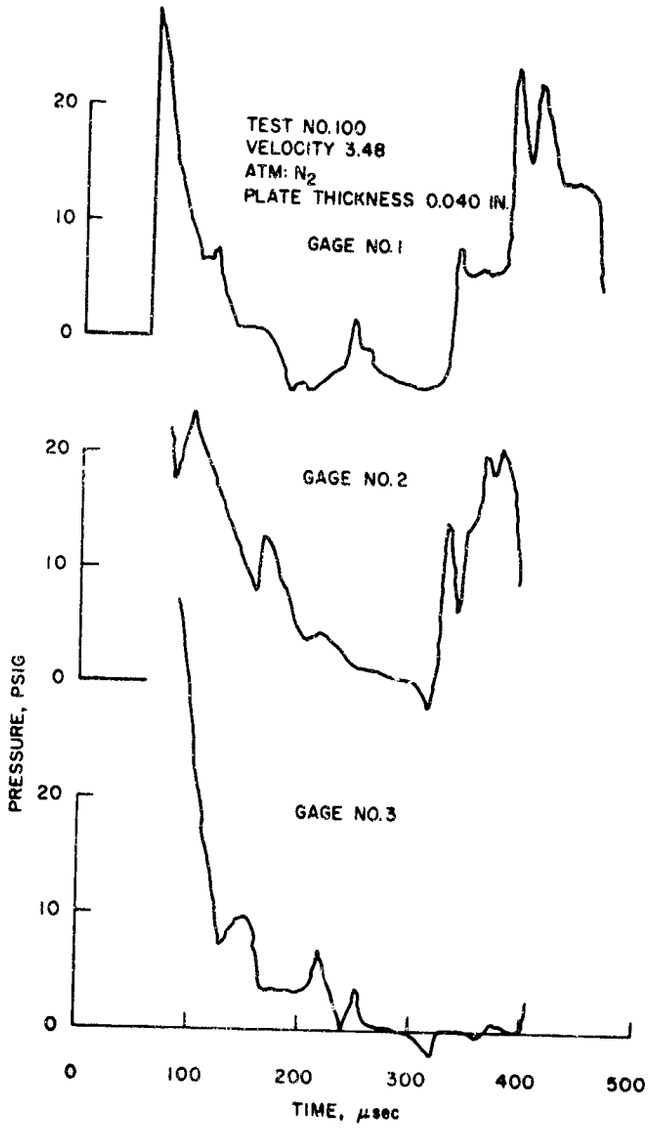
TEST NO. 100
VELOCITY 3.48
ATM: N_2
PLATE THICKNESS 0.040 IN.
GAGE NO. 1
GAGE NO. 2
GAGE NO. 3
PRESSURE, PSIG
TIME, μsec
0
10
20
100
200
300
400
500

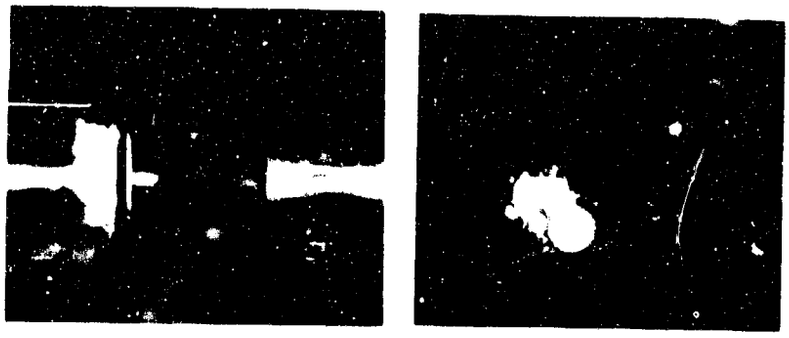

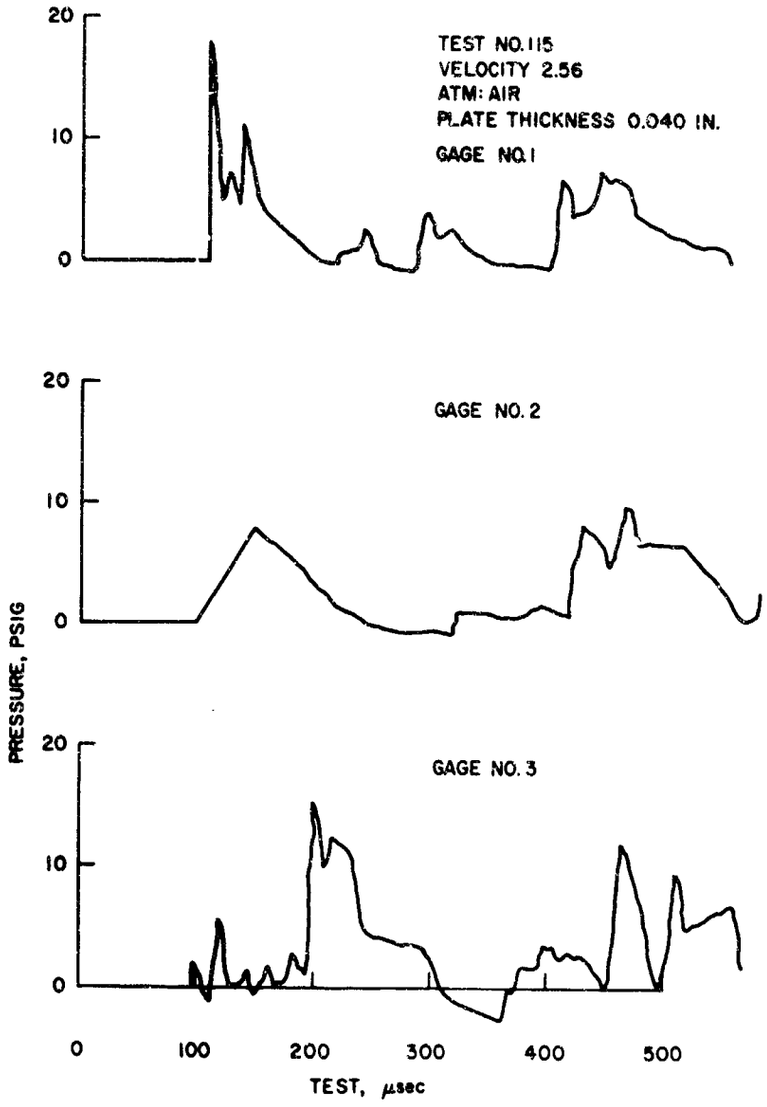
TEST NO. 115
VELOCITY 2.56
ATM: AIR
PLATE THICKNESS 0.040 IN.
GAGE NO. 1
GAGE NO. 2
GAGE NO. 3
PRESSURE, PSIG
20
10
0
0
100
200
300
400
500
TEST, μsec

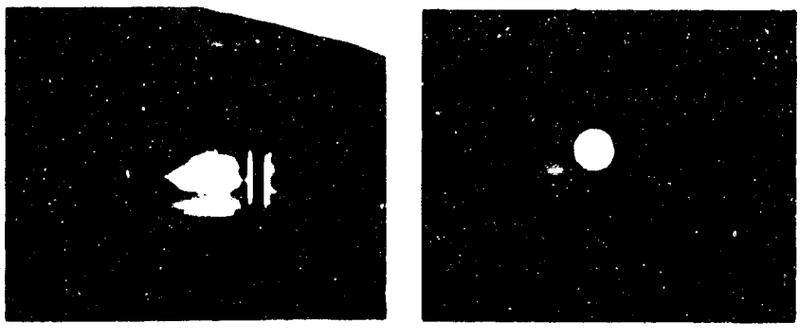

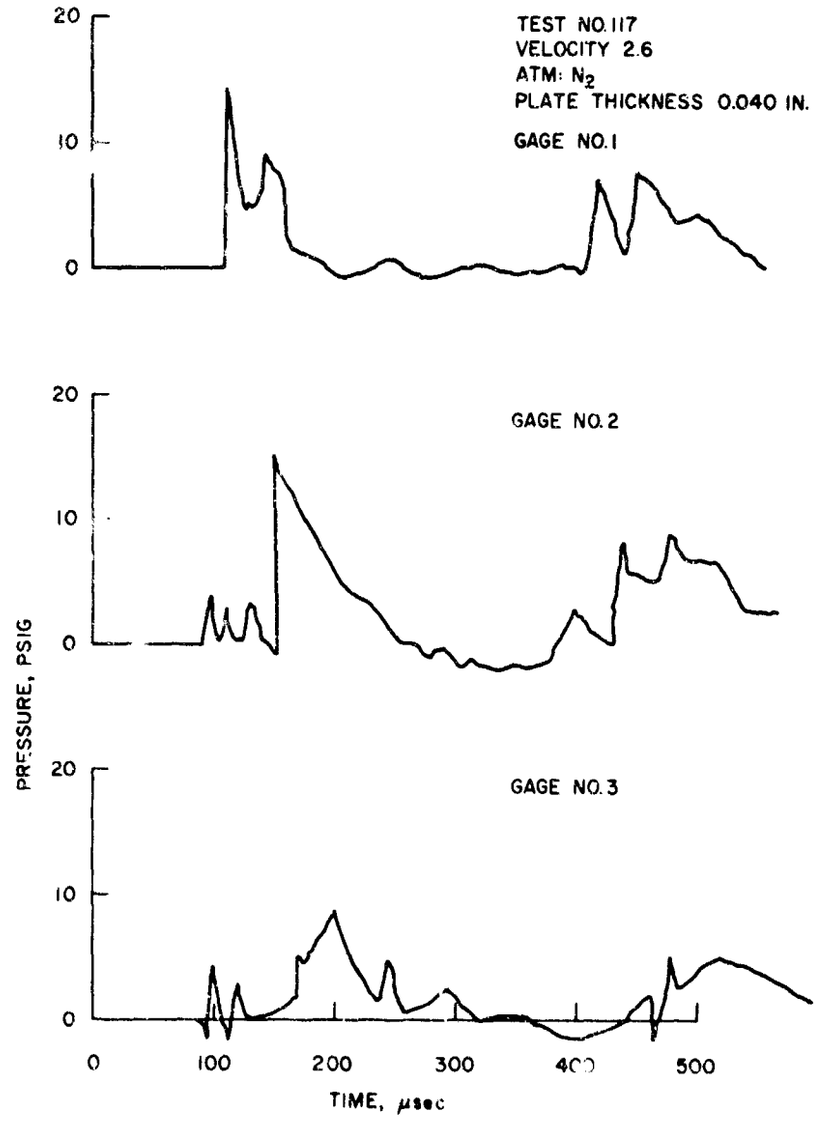
TEST NO.117
VELOCITY 2.6
ATM: N_2
PLATE THICKNESS 0.040 IN.
GAGE NO.1
GAGE NO.2
GAGE NO.3
PRESSURE, PSIG
20
10
0
0
100
200
300
400
500
TIME, μsec

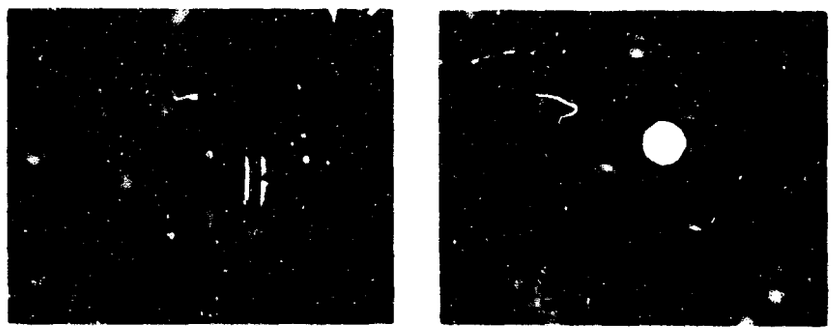

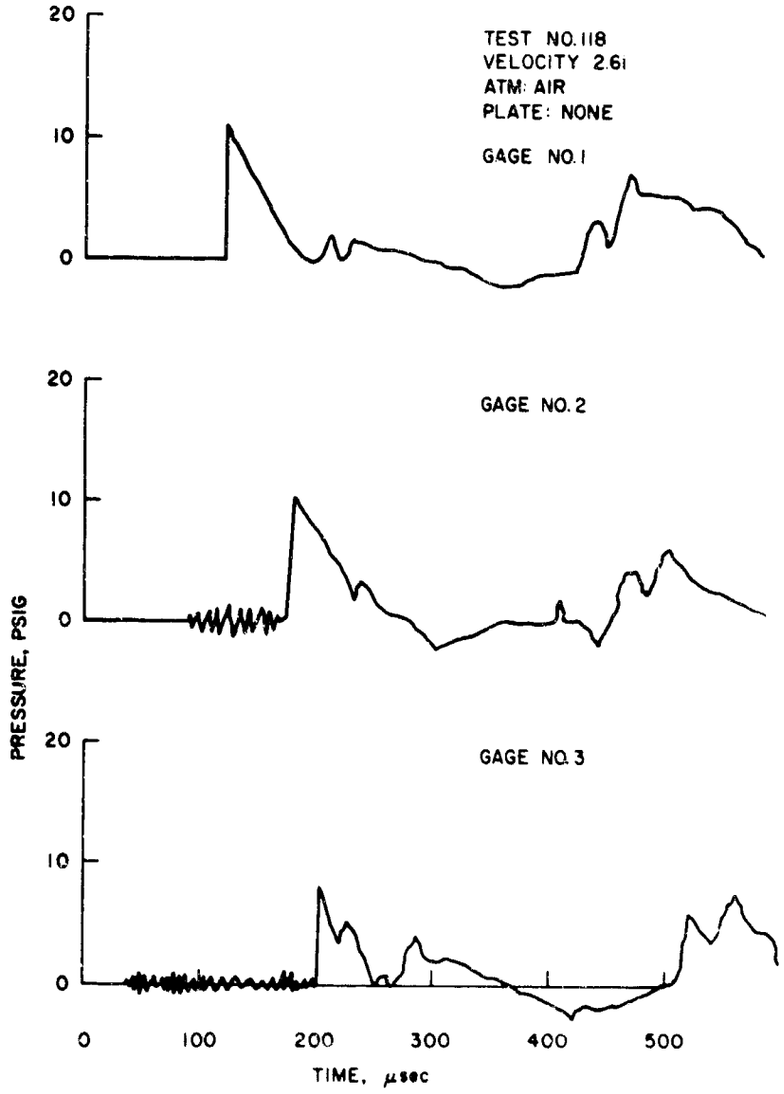

(No photographic data.)

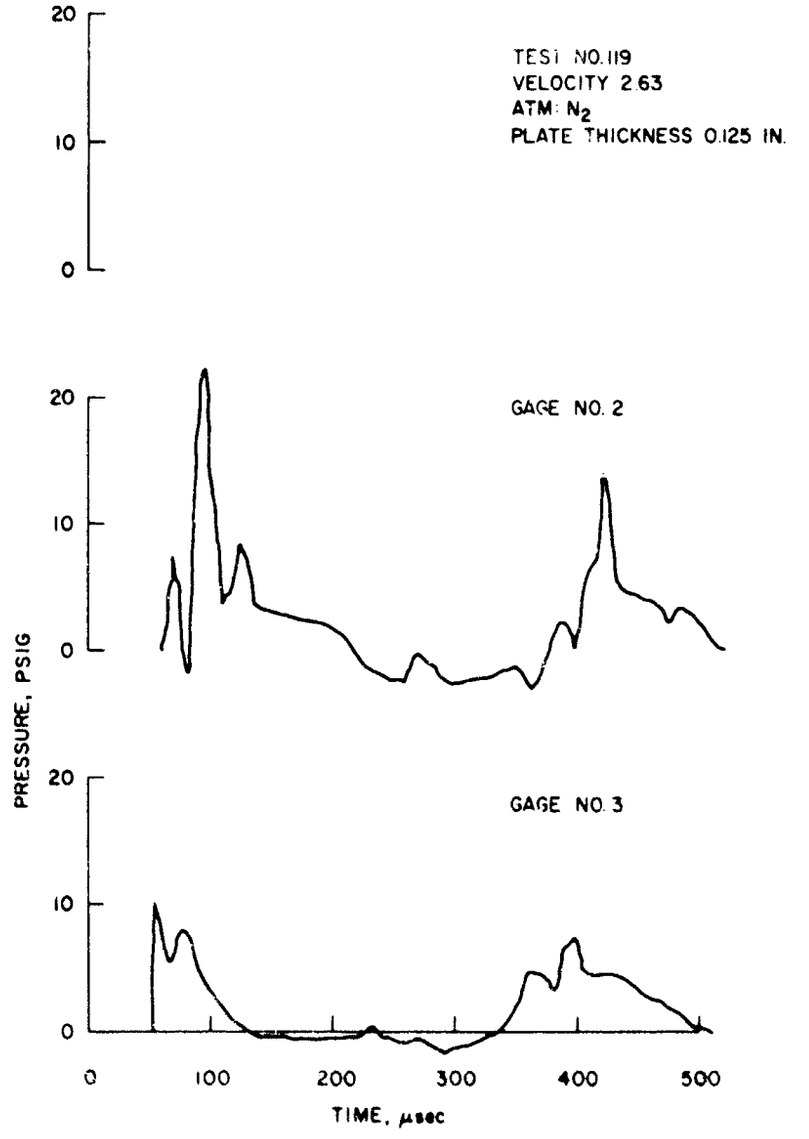
TEST NO.119
VELOCITY 2.63
ATM: N_2
PLATE THICKNESS 0.125 IN.
GAGE NO. 2
GAGE NO. 3
PRESSURE, PSIG
TIME, μsec
0
10
20
0
100
200
300
400
500

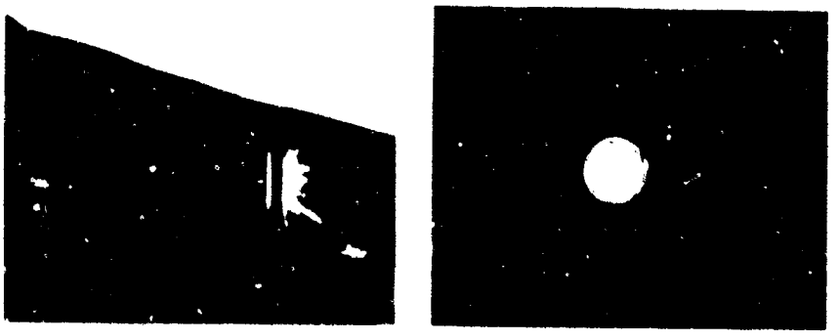

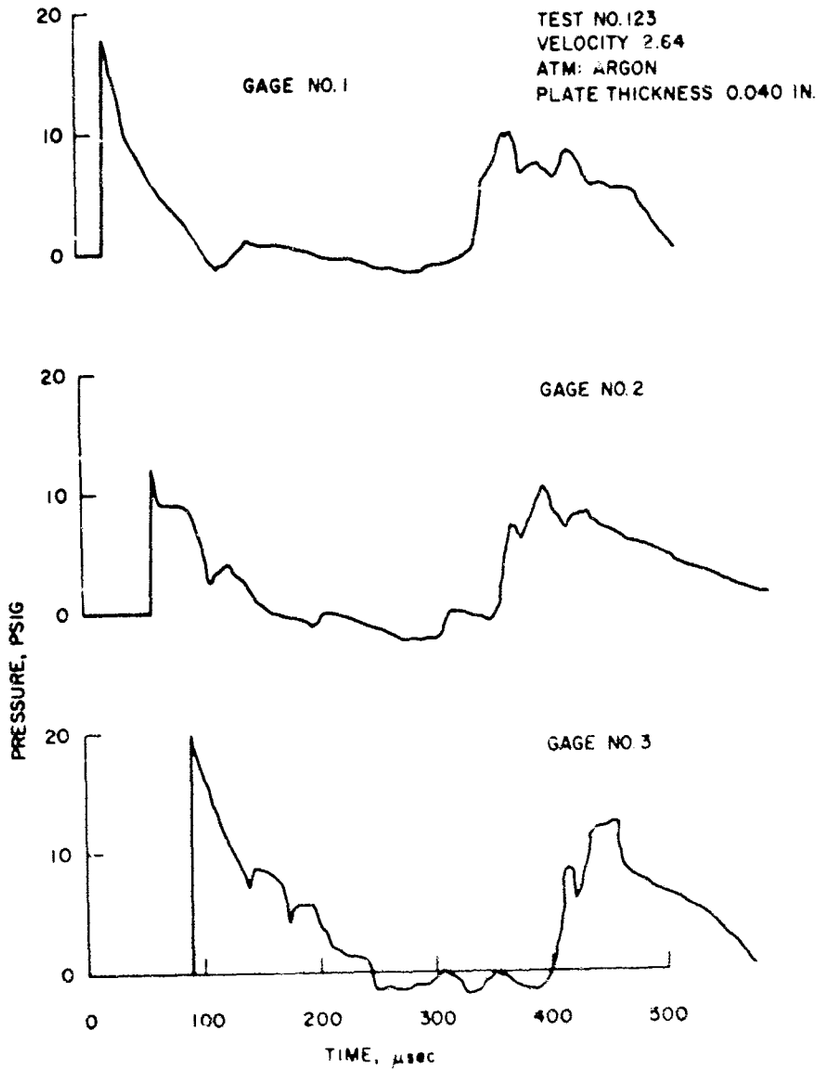
TEST NO. 123
VELOCITY 2.64
ATM: ARGON
PLATE THICKNESS 0.040 IN.
GAGE NO. 1
GAGE NO. 2
GAGE NO. 3
20
10
0
PRESSURE, PSIG
0
100
200
300
400
500
TIME, μsec

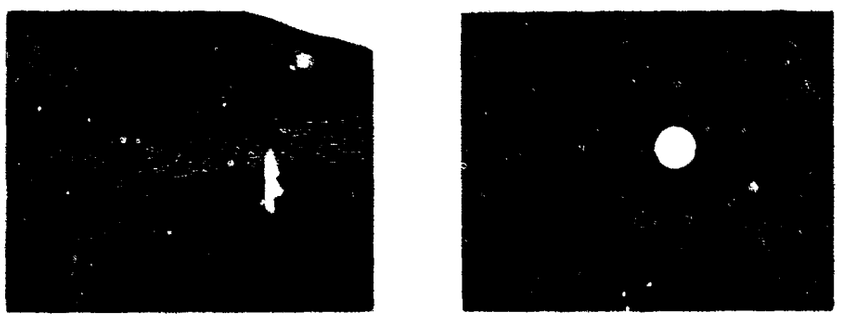

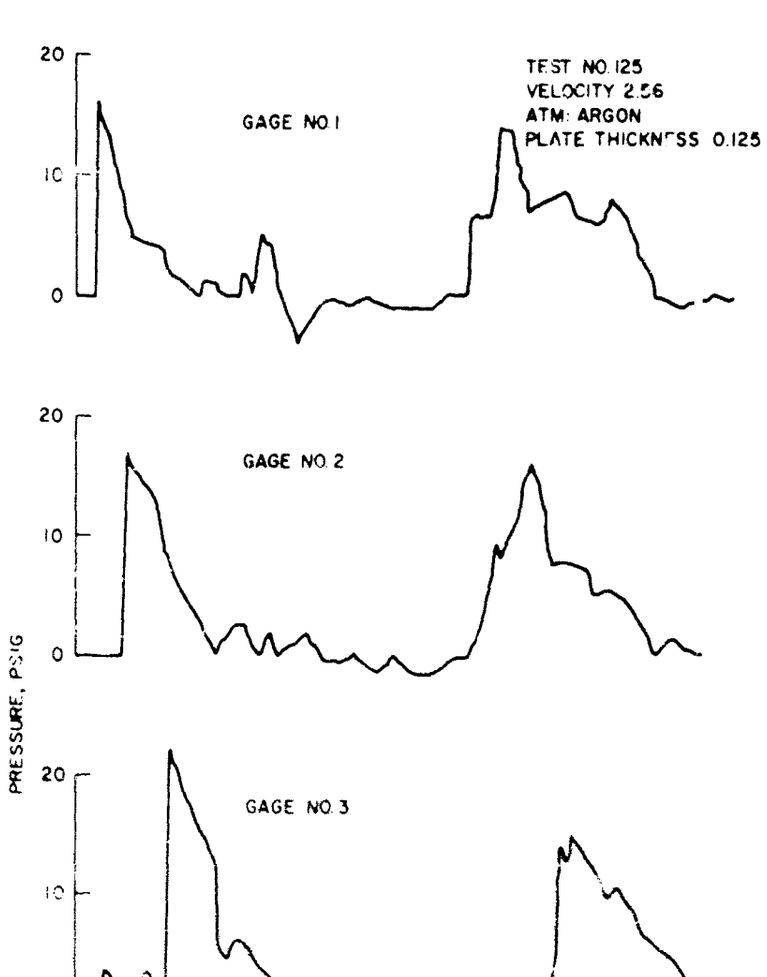
TEST NO. 125
VELOCITY 2.56
ATM: ARGON
PLATE THICKNESS 0.125
GAGE NO. 1
GAGE NO. 2
GAGE NO. 3
20
10
0
PRESSURE, PSIG
0
100
200
300
400
500
TIME, μsec

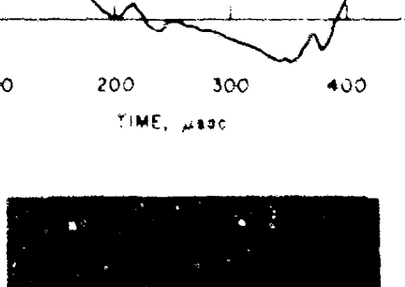

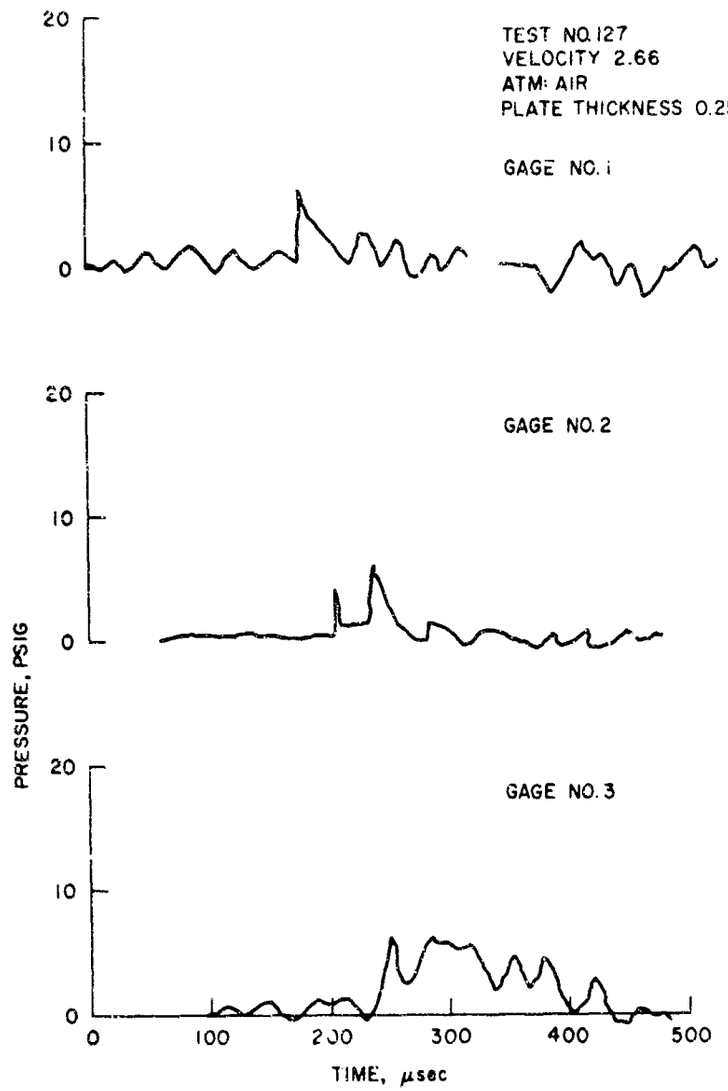
TEST NO.127
VELOCITY 2.66
ATM: AIR
PLATE THICKNESS 0.250 IN.
GAGE NO. 1
GAGE NO. 2
GAGE NO. 3
20
10
0
PRESSURE, PSIG
0
100
200
300
400
500
TIME, μsec

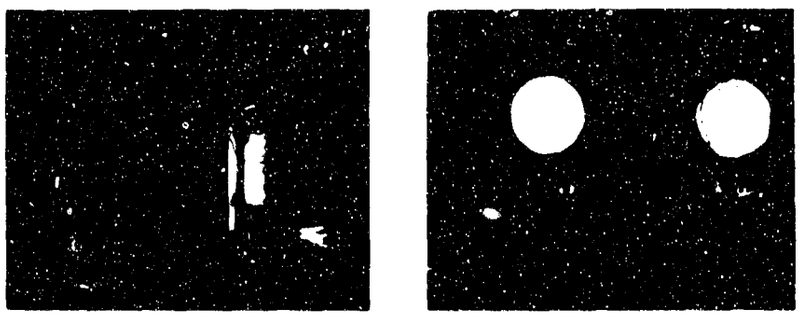

REF ENCES

1. U. S. Naval Ordnance Test Station. "Studies of Perforating Impacts at High Velocity," by M. E. Backman, in Transactions of the Symposium on Warhead Research (Surface Targets) 17-18 April 1962 (U). China Lake, Calif., NOTS, September 1962. (NOTS TP 2958), CONFIDENTIAL. Pp. 220-34

2. ------. "Measurements of the Atmospheric Disturbances Produced After the Perforation of a Thin Plate by a High-Speed Particle," by M. E. Backman, in Transactions of the Symposium on Warhead Research, 7-8 May 1963 (U). China Lake, Calif., NOTS, August 1963. (NOTS TP 3301), CONFIDENTIAL.

3. ------. "Energy Transferred to the Atmosphere by Fragment System of Various Distributions of Particle Size and Velocity," by M. E. Backman, in Transactions of the Third Symposium on Warhead Research, 5-7 May 19[illegible] (U). China Lake, Calif., NOTS, August 1964. (NOTS TP 3624), CONFIDENTIAL. Pp. 4-20.

4. Maiden, C. J. "Experimental and Theoretical Results Concerning the Protective Ability of a Thin Shield Against Hypervelocity Projectiles," PROC 6th SYMP HYPERVELOCITY IMPACT, CLEVELAND, Vol. III (August 1963), pp. 69-156.

5. Halperson, S. M. "Some Phenomena Associated with Impacts into Aluminum," PROC 6th SYMP HYPERVELOCITY IMPACT, CLEVELAND, Vol. III (August 1963), p. 539.

6. Herdan, G. Small Particle Statistics. Houston, Elsevier, 1953. P. 440.

7. Carnegie Institute of Technology. Spacial Distribution of Fragments Behind Thin Targets, by R. K. Becker and R. Vitali. Pittsburgh, Penn., CIT, October 1961. (24th Quarterly Progress Report.) Pp. 19 and 39.

8. Watson, R. W., K. R. Becker, and F. C. Gibson. "Thin Plate Perforation Studies With Projectiles in the Velocity Range From 2 to 5 km/sec," PROC 6th SYMP HYPERVELOCITY IMPACT, CLEVELAND, Vol. III (August 1963), p. 242.

9. General Motors Defense Research Laboratories. Investigation of Fundamental Mechanism of Damage of Thin Targets by Hypervelocity Projectiles, by C. J. Maiden, J. W. Gehring, and A. R. McMillan. Santa Barbara, Calif., GMDRL, 1963. (Report No. TR 63-225), p. 79.

10. Wolfhard, Hans G., Irvin Glassman, and Leon Green, Jr., eds. Heterogeneous Combustion (Progress in Astronautics and Aeronautics, Vol. 15). New York, Academic Press, 1964.

11. Markstein, G. H. "Combustion of Metals," AIAA J, Vol. 1, No. 3 (1963), pp. 551-62.

12. U. S. Naval Ordnance Test Station. Aluminum Particle Combustion Progress Report, 1 April 1964-30 June 1965, by Metal Combustion Study Group. China Lake, Calif., NOTS, April 1966. (Technical Progress Report 415, NOTS TP 3916).

13. Brzustowski, Thomas A., and Irvin Glassman. "Vapor Phase Diffusion Flames in the Combustion of Magnesium and Aluminum," in Heterogeneous Combustion (Progress in Astronautics and Aeronautics, Vol. 15), ed. by Hans G. Wolfhard, Irvin Glassman, and Leon Green, Jr. New York, Academic Press, 1964. Pp. 75-158.

14. Farber, M. "Thermodynamics of Al_2O_3," JET PROPULSION (November 1958), pp. 761-62.

15. Mellor, Arthur M., and Irvin Glassman. "Vapor-Phase Diffusion Flames in the Combustion of Magnesium and Aluminum: III. Experimental Observations in Carbon Dioxide Atmospheres," in Heterogeneous Combustion (Progress in Astronautics and Aeronautics, Vol. 15), ed. by Hans G. Wolfhard, Irvin Glassman, and Leon Green, Jr. New York, Academic Press, 1964. Pp. 159-73.

16. White, W. C. "Ablation from Aluminum Ultraspeed Pellets," ASTROPHYS J, Vol. 122, No. 3 (1955), pp. 559-64.

17. U. S. Naval Ordnance Test Station. Dynamics of Hypervelocity ($2\frac{1}{2}$ km/sec to 6 km/sec) Missiles, by J. S. Rinehart. China Lake, Calif., NOTS, July 1952. (NOTS TM 923).

18. Institute of Metals and Explosives Research, University of Utah. Observations of Vaporization Accompanying Ultra-high Velocity Impact, by R. W. Bartlett. Salt Lake City, Utah, IMER, January 1960. (OSR-TN-60-327.)

19. Rautenberg, T. H., and P. D. Johnson. "Light Production in the Aluminum-Oxygen Reaction," OPT SOC AM, J, Vol. 50, No. 6 (1960), pp. 602-06.

20. University of Utah. Hypervelocity Impact Spray Particles, by W. H. Clark, R. R. Kadesch, and R. W. Grow. Salt Lake City, Utah, 1960. (Technical Report OSR-18, Contract AF 49(638)-462.

21. White, W. C. "Suppression of AlO in the Wake of Ultraspeed Pellets," ASTROPHYS J, Vol. 121, No. 1 (1955), pp. 271-76.

22. Rinehart, J. S. "Simultaneous Photography of Self-Luminous and Non-Self-Luminous Events," REV SCI INSTR, Vol. 21, No. 11 (1950), pp. 939-40.

23. Friedman, R., and A. Macek. "Combustion Studies of Single Aluminum Particles," in Ninth Symposium (International) on Combustion. New York, Academic Press, 1963. Pp. 703-12.

24. Bartlett, R. W., J. N. Ong, W. M. Fassel, and C. A. Papp. "Estimating Aluminum Particle Combustion Kinetics," COMBUST FLAME, Vol. 7, No. 9 (1963), pp. 227-34.

25. Davis, A. "Solid Propellants: The Combustion of Particles of Metal Ingredients," COMBUST FLAME, Vol. 7, No. 12 (1963), pp. 359-67.

INITIAL DISTRIBUTION

12 Naval Air Systems Command
- AIR-302 (1)
- AIR-350 (1)
- AIR-350D (1)
- AIR-5108 (1)
- AIR-5321 (1)
- AIR-5323 (2)
- AIR-5324 (1)
- AIR-53242 (1)
- AIR-533 (1)
- AIR-604 (2)

5 Chief of Naval Operations
- OP-03EG (2)
- OP-05 (1)
- OP-55 (1)

8 Naval Ordnance Systems Command
- ORD-031 (1)
- ORD-034 (1)
- ORD-03521 (2)
- ORD-622 (2)
- ORD-9132 (2)

3 Office of Naval Research
- Code 104 (1)
- Code 429 (1)
- Code 461 (1)

1 Air Development Squadron 5
1 Fleet Anti-Air Warfare Training Center, San Diego
1 Marine Air Base Squadron 32
1 Marine Corps Air Station, Beaufort
1 Naval Air Engineering Center, Philadelphia
1 Naval Air Force, Atlantic Fleet
2 Naval Air Force, Pacific Fleet
2 Naval Air Mobile Training, Naval Air Station, Miramar
- Naval Air Mobile Training Detachment, 4003 Ordnance (1)
- Naval Air Mobile Training Detachment, 4030 Missile (1)

1 Naval Air Station, North Island
2 Naval Air Test Center, Patuxent River (Aeronautical Publications Library)
1 Naval Avionics Facility, Indianapolis (Technical Library)
1 Naval Explosive Ordnance Disposal Facility, Indian Head
1 Naval Missile Center, Point Mugu (Technical Library)
1 Naval Ordnance Laboratory, White Oak (Guided Missile Warhead Section)

UNCLASSIFIED
Security Classification

DOCUMENT CONTROL DATA · R&D

(Security classification of title, body of abstract and indexing annotation must be entered when the overall report is classified)

1. ORIGINATING ACTIVITY (Corporate author)	2a. REPORT SECURITY CLASSIFICATION
Naval Weapons Center China Lake, California 93555	UNCLASSIFIED
	2b. GROUP None

3. REPORT TITLE

PENETRATION MECHANICS AND POST-PERFORATION EFFECTS IN AN ALUMINUM-ALUMINUM IMPACT SYSTEM

4. DESCRIPTIVE NOTES *(Type of report and inclusive dates)*

Research Report

5. AUTHOR(S) *(Last name, first name, initial)*

Backman, Marvin E.; Stronge, William J.

6. REPORT DATE	7a. TOTAL NO. OF PAGES	7b. NO. OF REFS
October 1967	58	25

8a. CONTRACT OR GRANT NO.	9a. ORIGINATOR'S REPORT NUMBER(S)
b. PROJECT NO.	NWC TP 4414
c. NAVAIR A35-350-004/a16-1/F008-08-06.	9b. OTHER REPORT NO(S) *(Any other numbers that may be assigned this report)*
d.	

10. AVAILABILITY/LIMITATION NOTICES

This document has been approved for public release and sale; its distribution is unlimited.

11. SUPPLEMENTARY NOTES	12. SPONSORING MILITARY ACTIVITY
	Naval Air Systems Command Department of the Navy Washington, D. C. 20360

13. ABSTRACT

The perforation of 0.040-, 0.125-, and 0.250-inch 2024-T3 aluminum alloy plates by 0.063-, 0.125-, and 0.281-inch 2024-T8 aluminum spheres are investigated for the impact velocity range from 1.0 to 4.0 km/sec. The object of the investigation is to determine the mechanism of the formation of fragments, the distribution of fragment velocities and sizes, and the relation of atmospheric disturbances to these properties of the fragment system. The projectiles are launched from a conventional powder gun and from a light-gas gun both of which are 0.5 inch in barrel diameter. The investigation uses an Electro-Optics Kerr cell camera, paraffin and celotex techniques of particle recovery, and measurements of momentum by a ballistic pendulum. Pressures of atmospheric disturbances are estimated from highspeed photographs of the shocks and directly by piezoelectric gages mounted in the top of a box to which the target plate is mounted. Pressure measurements are found to correlate in a general way to the kinetic energy of the particle system but show no significant contribution from the combustion of aluminum in air. The pressures from 0.125- and 0.040-inch targets are essentially the same.

DD FORM 1 JAN 64 1473 0101-807-6800

UNCLASSIFIED
Security Classification

UNCLASSIFIED
Security Classification

14 KEY WORDS	LINK A		LINK B		LINK C	
	ROLE	WT	ROLE	WT	ROLE	WT
Penetration mechanics Post-perforation effects Al-Al impact system "Vaporifics" Aluminum combustion in impact						

INSTRUCTIONS

1. ORIGINATING ACTIVITY: Enter the name and address of the contractor, subcontractor, grantee, Department of Defense activity or other organization *(corporate author)* issuing the report.

2a. REPORT SECURITY CLASSIFICATION: Enter the overall security classification of the report. Indicate whether "Restricted Data" is included. Marking is to be in accordance with appropriate security regulations.

2b. GROUP: Automatic downgrading is specified in DoD Directive 5200.10 and Armed Forces Industrial Manual. Enter the group number. Also, when applicable, show that optional markings have been used for Group 3 and Group 4 as authorized.

3. REPORT TITLE: Enter the complete report title in all capital letters. Titles in all cases should be unclassified. If a meaningful title cannot be selected without classification, show title classification in all capitals in parenthesis immediately following the title.

4. DESCRIPTIVE NOTES: If appropriate, enter the type of report, e.g., interim, progress, summary, annual, or final. Give the inclusive dates when a specific reporting period is covered.

5. AUTHOR(S): Enter the name(s) of author(s) as shown on or in the report. Enter last name, first name, middle initial. If military, show rank and branch of service. The name of the principal author is an absolute minimum requirement.

6. REPORT DATE: Enter the date of the report as day, month, year; or month, year. If more than one date appears on the report, use date of publication.

7a. TOTAL NUMBER OF PAGES: The total page count should follow normal pagination procedures, i.e., enter the number of pages containing information.

7b. NUMBER OF REFERENCES: Enter the total number of references cited in the report.

8a. CONTRACT OR GRANT NUMBER: If appropriate, enter the applicable number of the contract or grant under which the report was written.

8b, 8c, & 8d. PROJECT NUMBER: Enter the appropriate military department identification, such as project number, subproject number, system numbers, task number, etc.

9a. ORIGINATOR'S REPORT NUMBER(S): Enter the official report number by which the document will be identified and controlled by the originating activity. This number must be unique to this report.

9b. OTHER REPORT NUMBER(S): If the report has been assigned any other report numbers *(either by the originator or by the sponsor)*, also enter this number(s).

10. AVAILABILITY/LIMITATION NOTICES: Enter any limitations on further dissemination of the report, other than those imposed by security classification, using standard statements such as:

(1) "Qualified requesters may obtain copies of this report from DDC."

(2) "Foreign announcement and dissemination of this report by DDC is not authorized."

(3) "U. S. Government agencies may obtain copies of this report directly from DDC. Other qualified DDC users shall request through _____."

(4) "U. S. military agencies may obtain copies of this report directly from DDC. Other qualified users shall request through _____."

(5) "All distribution of this report is controlled. Qualified DDC users shall request through _____."

If the report has been furnished to the Office of Technical Services, Department of Commerce, for sale to the public, indicate this fact and enter the price, if known.

11. SUPPLEMENTARY NOTES: Use for additional explanatory notes.

12. SPONSORING MILITARY ACTIVITY: Enter the name of the departmental project office or laboratory sponsoring *(paying for)* the research and development. Include address.

13. ABSTRACT: Enter an abstract giving a brief and factual summary of the document indicative of the report, even though it may also appear elsewhere in the body of the technical report. If additional space is required, a continuation sheet shall be attached.

It is highly desirable that the abstract of classified reports be unclassified. Each paragraph of the abstract shall end with an indication of the military security classification of the information in the paragraph, represented as *(TS)*, *(S)*, *(C)*, or *(U)*.

There is no limitation on the length of the abstract. However, the suggested length is from 150 to 225 words.

14. KEY WORDS: Key words are technically meaningful terms or short phrases that characterize a report and may be used as index entries for cataloging the report. Key words must be selected so that no security classification is required. Identifiers, such as equipment model designation, trade name, military project code name, geographic location, may be used as key words but will be followed by an indication of technical context. The assignment of links, roles, and weights is optional.

UNCLASSIFIED
Security Classification

ABSTRACT CARD

Naval Weapons Center
Penetration Mechanics and Post-Perforation Effects in an Aluminum-Aluminum Impact System, by Marvin E. Backman and William J. Stronge. China Lake, Calif., NOTS, October 1967. 58 pp. (NWC TP 4414), UNCLASSIFIED.

(Over)
2 cards, 8 copies

Naval Weapons Center
Penetration Mechanics and Post-Perforation Effects in an Aluminum-Aluminum Impact System, by Marvin E. Backman and William J. Stronge. China Lake, Calif., NOTS, October 1967. 58 pp. (NWC TP 4414), UNCLASSIFIED.

(Over)
2 cards, 8 copies

Naval Weapons Center
Penetration Mechanics and Post-Perforation Effects in an Aluminum-Aluminum Impact System, by Marvin E. Backman and William J. Stronge. China Lake, Calif., NOTS, October 1967. 58 pp. (NWC TP 4414), UNCLASSIFIED.

(Over)
2 cards, 8 copies

Naval Weapons Center
Penetration Mechanics and Post-Perforation Effects in an Aluminum-Aluminum Impact System, by Marvin E. Backman and William J. Stronge. China Lake, Calif., NOTS, October 1967. 58 pp. (NWC TP 4414), UNCLASSIFIED.

(Over)
2 cards, 8 copies

NWC TP 4414

ABSTRACT. The perforation of 0.040-, 0.125-, and 0.250-inch 2024-T3 aluminum alloy plates by 0.063-, 0.125-, and 0.281-inch 2024-T8 aluminum spheres are investigated for the impact velocity range from 1.0 to 4.0 km/sec. The object of the investigation is to determine the mechanism of the formation of fragments, the distribution of fragment velocities and sizes, and the relation of atmospheric disturbances to these properties of the fragment system. The projectiles are launched from a conventional powder gun and from a light-gas gun both of which are 0.5 inch in barrel diameter. The investigation uses an Electro-Optics

(Contd. on Card 2)

NWC TP 4414

ABSTRACT. The perforation of 0.040-, 0.125-, and 0.250-inch 2024-T3 aluminum alloy plates by 0.063-, 0.125-, and 0.281-inch 2024-T8 aluminum spheres are investigated for the impact velocity range from 1.0 to 4.0 km/sec. The object of the investigation is to determine the mechanism of the formation of fragments, the distribution of fragment velocities and sizes, and the relation of atmospheric disturbances to these properties of the fragment system. The projectiles are launched from a conventional powder gun and from a light-gas gun both of which are 0.5 inch in barrel diameter. The investigation uses an Electro-Optics

(Contd. on Card 2)

NWC TP 4414

ABSTRACT. The perforation of 0.040-, 0.125-, and 0.250-inch 2024-T3 aluminum alloy plates by 0.063-, 0.125-, and 0.281-inch 2024-T8 aluminum spheres are investigated for the impact velocity range from 1.0 to 4.0 km/sec. The object of the investigation is to determine the mechanism of the formation of fragments, the distribution of fragment velocities and sizes, and the relation of atmospheric disturbances to these properties of the fragment system. The projectiles are launched from a conventional powder gun and from a light-gas gun both of which are 0.5 inch in barrel diameter. The investigation uses an Electro-Optics

(Contd. on Card 2)

NWC TP 4414

ABSTRACT. The perforation of 0.040-, 0.125-, and 0.250-inch 2024-T3 aluminum alloy plates by 0.063-, 0.125-, and 0.281-inch 2024-T8 aluminum spheres are investigated for the impact velocity range from 1.0 to 4.0 km/sec. The object of the investigation is to determine the mechanism of the formation of fragments, the distribution of fragment velocities and sizes, and the relation of atmospheric disturbances to these properties of the fragment system. The projectiles are launched from a conventional powder gun and from a light-gas gun both of which are 0.5 inch in barrel diameter. The investigation uses an Electro-Optics

(Contd. on Card 2)